

1 **Normal mitochondrial function in *Saccharomyces cerevisiae* has become**  
2 **dependent on inefficient splicing**

3

4 Marina Rudan<sup>1</sup>, Peter Bou Dib<sup>2</sup>, Marina Musa<sup>1</sup>, Matea Kanunnikau<sup>1</sup>, Sandra  
5 Sobočanec<sup>3</sup>, David Rueda<sup>4,5,6</sup>, Tobias Warnecke<sup>4,5\*</sup>, Anita Kriško<sup>1\*</sup>

6

7 <sup>1</sup>Mediterranean Institute for Life Sciences, Meštrovićevo šetalište 45, 21000 Split,  
8 Croatia

9 <sup>2</sup>Universitätsmedizin Göttingen, Institut für Zellbiochemie, Humboldtallee 23, 37073  
10 Göttingen

11 <sup>3</sup>Division of Molecular Medicine, Rudjer Boškovic Institute, Bijenička 54, 10000  
12 Zagreb, Croatia

13 <sup>4</sup>MRC London Institute of Medical Sciences (LMS), Du Cane Road, London W12  
14 0NN, United Kingdom

15 <sup>5</sup>Institute of Clinical Sciences (ICS), Faculty of Medicine, Imperial College London,  
16 Du Cane Road, London W12 0NN, United Kingdom

17 <sup>6</sup>Molecular Virology, Faculty of Medicine, Imperial College London, Du Cane Road,  
18 London W12 0NN, United Kingdom

19

20 Running title: Inefficient splicing at the heart of mitochondrial function

21

22 \*co-corresponding authors

23 **Self-splicing introns are mobile elements that have invaded a number of highly**  
24 **conserved genes in prokaryotic and organellar genomes. Here, we show that**  
25 **deletion of these selfish elements from the *Saccharomyces cerevisiae***  
26 **mitochondrial genome is stressful to the host. A strain without mitochondrial**  
27 **introns displays hallmarks of the retrograde response, with altered**  
28 **mitochondrial morphology, gene expression and metabolism impacting growth**  
29 **and lifespan. Deletion of the complete suite of mitochondrial introns is**  
30 **phenocopied by overexpression of the splicing factor Mss116. We show that, in**  
31 **both cases, abnormally efficient transcript maturation results in excess levels of**  
32 **mature *cob* and *cox1* host mRNA. Thus, inefficient splicing has become an**  
33 **integral part of normal mitochondrial gene expression. We propose that the**  
34 **persistence of *S. cerevisiae* self-splicing introns has been facilitated by an**  
35 **evolutionary lock-in event, where the host genome adapted to primordial**  
36 **invasion in a way that incidentally rendered subsequent intron loss deleterious.**

37

38 Mobile genetic elements frequently compromise host fitness<sup>1</sup>, corrupting genetic  
39 information or disturbing adaptive gene expression patterns, sometimes to lethal  
40 effect. Despite this, mobile genetic elements are ubiquitous in most eukaryotic  
41 genomes<sup>2</sup>. How do these selfish elements persist in a genomic environment where –  
42 even in the absence of selection – mutational forces constantly work to erode them?  
43 Although mobile elements can donate motifs (or domains) that are co-opted into host  
44 regulatory pathways (or genic sequence) over time<sup>3</sup>, deletions usually whittle away all  
45 but the core beneficial motif. The components that once mediated mobility, such as  
46 the reverse transcriptases of long interspersed nuclear elements (LINEs), are typically  
47 lost. Thus, functional selfish elements that remain mobile are thought to persist over

48 evolutionary time not by virtue of sporadic beneficial effects for the host, but because  
49 they replicate and spread to other sites in the genome faster than they are deleted<sup>3</sup>.

50 The element survives, not where it originally invaded but as a descendant copy  
51 elsewhere in the genome.

52

53 An interesting exception in this regard are self-splicing introns, which populate some  
54 highly expressed genes in archaea, bacteria, and organellar genomes of fungi and  
55 plants<sup>4</sup>. In contrast to other mobile elements, self-splicing introns do not spawn a  
56 large pool of copies that disperse across the genome to escape mutational erasure.

57 Rather, owing to highly specific homing sites, each intron is typically confined to a  
58 single location in the host genome and evolutionary persistence seems to rely on  
59 continued re-invasion, either from other individuals in the same population<sup>5</sup> or across  
60 species boundaries<sup>6-8</sup>. Self-splicing introns can spread despite considerable fitness  
61 costs to the host<sup>9</sup>. However, in practice, fitness costs might be relatively low as the  
62 host RNA is intact and fully functional once the intron has been spliced out. As far as  
63 we know, self-splicing introns do not contribute positively to host fitness and, naively,  
64 one would expect that deleting these introns from the genome would be beneficial or,  
65 at worst, make no difference to the host.

66

67 Here, we investigate the consequences of deleting all 13 self-splicing introns from the  
68 *S. cerevisiae* mitochondrial genome, where they reside in three host genes: the 21S  
69 ribosomal RNA gene Q0158 (which harbours a single group I intron named *omega*)  
70 and two protein-coding genes, *cox1* (group I: aI3, aI4, aI5 $\alpha$ , aI5 $\beta$ ; group II: aI1, aI2,  
71 aI5 $\gamma$ ) and *cob* (group I: bI2, bI3, bI4, bI5; group II: bI1), both encoding components  
72 of the electron transport chain. Note here, that we use “self-splicing introns” as a

73 convenient shorthand to describe the complete collection of group I and group II  
74 introns, even though timely splicing *in vivo* often depends on one or several *trans*-  
75 factors (see below)<sup>4</sup>. We show that, contrary to expectations, removing these introns  
76 has dramatic consequences for mitochondrial physiology and function, triggering  
77 changes in nuclear gene expression that affect organismal growth and lifespan. Our  
78 results demonstrate that the presence of mitochondrial self-splicing introns has  
79 become integral to normal mitochondrial gene expression and that, curiously, normal  
80 mitochondrial function in *S. cerevisiae* has come to require inefficient splicing. Our  
81 findings have implications for understanding how self-splicing introns and mobile  
82 elements more generally can survive over evolutionary time without providing an  
83 adaptive benefit to the host.

84

## 85 **Results**

86

87 *Removal of mitochondrial introns is associated with a multi-faceted stress phenotype*

88

89 To test whether the removal of self-splicing mitochondrial introns affects host  
90 physiology and fitness, we compared two *S. cerevisiae* strains that are isogenic with  
91 regard to their nuclear genomes (except for a single marker gene, *ura3*, see Methods)  
92 but differ with respect to mitochondrial intron content. The control strain a161 (WT)  
93 contains the full complement of seven *cox1* and five *cob* introns, whereas strain a161-  
94 U7 (*I<sub>0</sub>*) carries an intronless mitochondrial genome, which was originally constructed  
95 by Seraphin and co-workers via serial recombination of natural yeast isolates that lack  
96 individual mitochondrial introns<sup>10</sup>.

97

98 Contrary to a model where self-splicing introns are dispensable parasitic passengers,  
99 we find that *I<sub>0</sub>* exhibits stark phenotypic differences to the control strain. When the  
100 two strains are cultured in isolation, exponential growth on glucose-supplemented  
101 YPD medium is ~30% slower for *I<sub>0</sub>* compared to WT (Figure 1a). *I<sub>0</sub>* also fares poorly  
102 when pitted directly against WT in competitive fitness assay (Figure 1-figure  
103 supplement 1). Chronological life span (CLS, see Methods), on the other hand, is  
104 almost two-fold longer for *I<sub>0</sub>* (Figure 1b). At the cellular level, *I<sub>0</sub>* displays increased  
105 mitochondrial mass and volume and a mitochondrial morphology characterized by a  
106 large network of branched tubules of homogeneous diameter (Figure 1c-e). Transcript  
107 levels of mitofusin (*fzo1*) and the GTPase *mgm1*, key nuclear encoded regulators of  
108 mitochondrial fusion, are strongly upregulated (qPCR, *t*-test, *fzo1*: 4.02-fold, p=0.002;  
109 *mgm1*: 5.24-fold, p=3.19x10<sup>-5</sup>, Figure 2a) while levels of *dnm1* and *fis1*, which  
110 orchestrate mitochondrial fission, are only moderately induced (qPCR, *t*-test, *dnm1*:  
111 1.67-fold, p=0.026; *dnm1*: 1.81-fold, p=0.085), suggesting that the changes in  
112 mitochondrial morphology result from increased fusion rather than impaired fission.  
113 The *I<sub>0</sub>* strain also exhibits a 2.7-fold increase in mitochondrial DNA copy number  
114 (qPCR, *t*-test P=1.09x10<sup>-7</sup>). At the same time, there are no significant differences in  
115 mitochondrial inner membrane potential, as measured by 3,3'-  
116 Dihexyloxacarbocyanine iodide [DiOC6(3)] fluorescence (Figure 1f), suggesting that  
117 mitochondria are functional despite grossly altered morphology. This notion is further  
118 supported by the observation that *I<sub>0</sub>* retains the capacity to grow on glycerol, a non-  
119 fermentable carbon source (Figure 1-figure supplement 2), as previously reported for  
120 a different nuclear background<sup>11</sup>. In fact, biomarkers of mitochondrial metabolism  
121 point to increased mitochondrial activity, with higher oxygen consumption (Figure  
122 1g) and cellular ATP levels (Figure 1h) during exponential growth. Despite increased

123 activity, levels of mitochondrial superoxide are reduced (Figure 1i), likely reflecting a  
124 >7.5-fold upregulation of the mitochondrial ROS-scavenger *sod2* (qPCR, *t*-test  
125  $P=0.003$ , Figure 2a). Thus, intron removal challenges but does not terminally  
126 compromise mitochondrial function.

127

### 128 *Removal of mitochondrial introns triggers the retrograde response*

129

130 The phenotypic changes we observe suggest an involvement of the retrograde  
131 response, as do upregulation of *cit2*, upregulation of the two rate-limiting members of  
132 the TCA cycle, *cit1* and *idh1*, and upregulation of both mitochondrially (*cox1*, *cox2*,  
133 *atp6*) and nuclearly (*cox4*, *atp1*, *sdh1*, *sdh2*) encoded parts of the respiratory chain  
134 (Figure 2a). Indeed, deletion of *rtg2*, the transcriptional master regulator of the  
135 retrograde response and a sensor of mitochondrial dysfunction, suppresses the *I<sub>o</sub>*  
136 phenotype (Figure 3). Tubular structure is lost and large spherical shapes become  
137 prominent (Figure 3a), suggesting distinct defects in the maintenance of  
138 mitochondrial ultrastructure<sup>12,13</sup>. Deletion of *rtg2* in WT strains, where the retrograde  
139 response is not activated, has no significant effect on mitochondrial volume and  
140 morphology, oxygen consumption and ATP levels (Figure 3a-d). The extension of  
141 CLS is abrogated in the absence of *rtg2*, becoming shorter even than the wildtype  
142 (Figure 3e). Upon deletion of *hap4*, the transcriptional activator of nuclearly encoded  
143 components of the respiratory chain (as well as the TCA cycle enzymes under normal  
144 conditions), mitochondrial morphology reverts back to the wild-type state (Figure 4a-  
145 e). We conclude that an intact retrograde response, including upregulation of nuclear  
146 components of the respiratory chain, is necessary to generate the mitochondrial  
147 phenotype observed in the *I<sub>o</sub>* strain.

148

149 *Promoter attenuation of cox1 and cob reverses the phenotype*

150

151 To determine the ultimate molecular trigger(s) of the retrograde response, we  
152 examined how intron removal affects host gene expression. As previous work had  
153 found the *omega* intron to be “optional” – present in some yeast strains but absent in  
154 others without obvious phenotypic effects<sup>14,15</sup> – we focused on *cox1* and *cob*. For both  
155 these genes, mRNA levels are strongly elevated in *I<sub>0</sub>* (10.9-fold and 5.8-fold for *cox1*  
156 and *cob*, respectively; Figure 2a) but also in  $\Delta$ *rtg2* (Figure 3f) and  $\Delta$ *hap4* (Figure 4f),  
157 suggesting that this is a direct effect of intron removal rather than a downstream  
158 consequence of activating the retrograde response. To investigate whether elevated  
159 *cox1* and/or *cob* transcript levels might underpin the wider transcriptional, metabolic  
160 and phenotypic changes, we introduced attenuating point mutations into the promoters  
161 of *cox1* and *cob* (see Methods). We find that simultaneous attenuation of both  
162 promoters in *I<sub>0</sub>* fully reverses the *I<sub>0</sub>*-characteristic suite of morphological and molecular  
163 phenotypes (see *I<sub>0pp</sub>* throughout Figure 5). Attenuation of either *cob* (*I<sub>0cobp</sub>*) or *cox1*  
164 (*I<sub>0cox1p</sub>*) in isolation only partially reverses the phenotype, although *I<sub>0cobp</sub>* has a  
165 larger relative effect than *I<sub>0cox1p</sub>* (Figure 5).

166

167 *The effects of intron removal are phenocopied by overexpression of Mss116*

168

169 Next, we sought to establish why the wholesale deletion of self-splicing introns leads  
170 to increased abundance of the host transcripts. We considered two main possibilities.  
171 First, in deleting introns, we might have inadvertently removed DNA-/RNA-level  
172 regulatory elements that affect expression of the host genes. Alternatively, the act of

173 short-circuiting the splicing process itself might interfere with normal expression.  
174 Specifically, we hypothesized that normal levels of transcription might be tuned to  
175 accommodate a certain proportion of transcripts that fail to splice correctly. Group II  
176 introns in particular are known for low splicing efficiency, even in the presence of  
177 auxiliary proteins<sup>16</sup>. As a corollary, a large fraction of pre-mRNAs might be targeted  
178 and degraded by mitochondrial quality control, either because splicing is erroneous  
179 (mis-splicing) or does not occur in a timely manner so that the transcript is shunted  
180 into degradation (kinetic coupling). In *I<sub>0</sub>*, splicing does not occur so that erroneous  
181 splicing products do not arise. As a result, production of functional *cox1/cob* mRNAs  
182 might overshoot its target and trigger a system-wide response, for example because  
183 altered COX1/COB levels upset dosage balance amongst respiratory complexes. To  
184 test this abnormally-efficient-maturation hypothesis and simultaneously rule out that  
185 mitochondrial stress is caused by the removal of DNA-/RNA-level regulatory  
186 elements, we sought to alter splicing efficiency by orthogonal means. To this end, we  
187 overexpressed the nuclearly encoded DEAD box RNA helicase Mss116, which  
188 promotes splicing of all *S. cerevisiae* mitochondrial introns by remodeling or  
189 stabilizing splice-relevant RNA structures in an ATP-dependent manner<sup>16,17</sup>. We  
190 confirmed overexpression and mitochondrial localization of Mss116 by flow  
191 cytometry and immunofluorescence, respectively, using an N-terminal His-tagged  
192 version of the protein (Figure 1-figure supplement 3), and then characterized the  
193 effects of Mss116 overexpression in the Y258 strain using an untagged version of the  
194 protein. Remarkably, the Mss116 overexpression strain (*MSS116<sub>OE</sub>*) phenocopies *I<sub>0</sub>*.  
195  
196 *MSS116<sub>OE</sub>* exhibits increased generation times, extended chronological life span,  
197 lower competitive fitness, increased mitochondrial fusion, 2.9-fold increased mtDNA

198 copy number (qPCR,  $t$ -test  $P=5.5 \times 10^{-7}$ ), elevated oxygen consumption, and altered  
199 ATP and ROS production (Figure 1, Figure 1-figure supplement 1). In addition, we  
200 observe longer replicative life span (RLS) in *MSS116<sup>OE</sup>* (Figure 1-figure supplement  
201 4), a more direct proxy of ageing that we were not able to measure accurately in *I<sub>0</sub>*,  
202 where separating mother and daughter cells in a timely fashion proved challenging  
203 (see Methods). Overexpression of a DEAD box mutant of Mss116 (*MSS116<sup>E268K</sup>*),  
204 which lacks ATPase and therefore helicase activity, does not phenocopy *I<sub>0</sub>* (Figure 1).  
205 This suggests that the role of Mss116 in splicing – which relies on helicase activity –  
206 is critical rather than a recently suggested ATP-independent role in transcription  
207 elongation<sup>18</sup>. More generally, the fact that *MSS116<sup>OE</sup>* – which encodes a full  
208 complement of introns – phenocopies *I<sub>0</sub>* indicates that the stress phenotype in these  
209 strains is not caused by missing DNA-level functionality and instead points towards a  
210 critical role for splicing. Overexpressing Mss116 in *I<sub>0</sub>* did not reveal additional  
211 phenotypes and the strain behaved like *I<sub>0</sub>* (Figure 2-figure supplement 1) further  
212 supporting the notion that intron deletion and Mss116 overexpression act through the  
213 same pathway.

214

215 *Cells are stressed because of abnormally efficient transcript maturation*

216

217 We suspected that phenotypic effects of Mss116 overexpression (and intron deletion)  
218 are linked to altered transcript maturation of the host genes, *cob* and *cox1*. However,  
219 we first wanted to rule out an alternative hypothesis. In both *MSS116<sup>OE</sup>* and *I<sub>0</sub>*,  
220 Mss116 is in excess relative to need (in *MSS116<sup>OE</sup>* because Mss116 is overexpressed,  
221 in *I<sub>0</sub>* because its usual targets – the introns – are absent). Phenotypic effects could  
222 therefore be caused by excess Mss116 interacting with RNAs that it would not

223 normally target or not target to the same extent. This is conceptually related to the  
224 idea that splicing dynamics can change simply as a result of altered competition  
225 between mRNAs for access to the spliceosome<sup>19</sup>. To test this hypothesis, we deleted  
226 *Mss116* in the *I<sub>0</sub>* strain. We observe the same suite of phenotypes we see in *I<sub>0</sub>* (Figure  
227 2-figure supplement 2), demonstrating that neither absolute nor relative excess of  
228 *Mss116* are responsible for the stress phenotype described above.

229

230 Having ruled out this hypothesis, we then focused on characterizing the effects of  
231 *Mss116* overexpression on *cob/cox1* splicing dynamics in greater detail. Using qPCR,  
232 we first measured the levels of total *cox1* and *cob* transcripts as well as individual  
233 introns at steady state (Figure 2a, 240 mins after *Mss116* induction, see Figure 2-  
234 figure supplement 3). For *cox1*, we additionally monitored exon and intron ( $\alpha 12$ ,  $\alpha 15\beta$ )  
235 levels using RNA fluorescent *in situ* hybridization (RNA FISH, Figure 2b, see  
236 Methods). We find that most mitochondrial introns are strongly depleted in *MSS116OE*  
237 compared to the empty vector control and relative to exons. The relative depletion of  
238 individual introns is somewhat variable and one intron –  $\alpha 15\alpha$  - is equally abundant in  
239 *MSS116OE* and the Y258 WT (Figure 2a). We then examined shifts in the abundance  
240 of pre-mRNA and mature mRNA over the course of *Mss116* induction, using  
241 different primer combinations to monitor unspliced RNAs and spliced exon-exon  
242 junctions. For both *cox1* and *cob*, *Mss116* overexpression shifts the balance between  
243 unspliced (or partially spliced) pre-mRNA transcripts, which dominate the uninduced  
244 steady state, towards mature mRNA transcripts (Figure 2c), while total transcript  
245 abundance (mRNA plus pre-mRNA) remains largely unchanged. These observations  
246 are consistent with a model where nascent transcriptional output is unchanged in

247 *Mss116OE* compared to the empty vector control and differential steady state levels  
248 are the result of post-transcriptional events.

249

250 Based on these findings, we suggest that *Mss116OE* phenocopies *I<sub>0</sub>* because  
251 eliminating introns at the DNA level (*I<sub>0</sub>*) and facilitating accurate and efficient  
252 excision at the RNA level (*Mss116OE*) both result in abnormally efficient transcript  
253 maturation. That is, fewer transcripts are eliminated by mitochondrial quality control  
254 because splicing is erroneous or does not proceed in a timely manner, resulting in a  
255 greater number of mature *cox1/cob* mRNAs. For reasons that remain to be elucidated,  
256 increased transcript levels are then perceived as stressful and trigger the retrograde  
257 response, culminating in a multifaceted stress phenotype. We speculate in this regard  
258 that elevated protein levels of COB (*I<sub>0</sub>*: 9.3-fold; *Mss116OE*: 5.0-fold upregulation, as  
259 determined by quantitative label-free mass spectrometry) and COX1 (*I<sub>0</sub>*: 11.6-fold;  
260 *Mss116OE*: 12.1-fold upregulation) might interfere with proper assembly and function  
261 of complex III and complex IV, respectively, and therefore constitute a deleterious  
262 dosage imbalance phenotype.

263

264

## 265 **Discussion**

266

267 It is now well documented that disruption of splicing homeostasis can impact normal  
268 physiological function and lead to cellular stress and disease<sup>20</sup>. There is also  
269 increasingly detailed mechanistic knowledge of how proteins involved in splicing can  
270 alter growth and ageing via a metabolic route, exemplified by the recent finding that  
271 splicing factor 1 is a modulator of dietary restriction-induced longevity in

272 *Caenorhabditis elegans*<sup>21</sup>. The classic model here is that loss of splicing homeostasis  
273 – through genetic, developmental, or environmental perturbation – leads to  
274 deleterious shifts in splice isoform production or precipitates increased production of  
275 erroneous transcripts that tax the quality control system and/or have direct cytotoxic  
276 effects. In other words, the disease/stress state is a high-error state. Our results are  
277 unusual in that they suggest that normal splicing can be associated with high error  
278 rates and that, therefore, splicing homeostasis can also be disturbed by increasing  
279 splicing efficacy.

280

281 Further research will be required to tease apart how individual mitochondrial introns  
282 affect the overall burden from failed splicing in this system. It is evident from  
283 population genomic analysis of different *S. cerevisiae* strains that some mitochondrial  
284 introns are fixed across extant populations whereas others exhibit presence/absence  
285 polymorphism<sup>14</sup>. This seems to suggest that the removal of at least some introns in  
286 isolation is insufficiently stressful to be purged by natural selection. At the same time,  
287 studies of *suv3*, the second DEAD box RNA helicase present in yeast mitochondria,  
288 suggest that the deleterious effect of deleting individual introns – while possibly  
289 idiosyncratic – is at least partially cumulative: deletion of *suv3*, a component of the  
290 mitochondrial degradosome, decreases levels of mature *cox1/cob* mRNA and  
291 compromises respiratory capacity, but less so where more introns had been removed  
292 from the mitochondrial DNA<sup>22</sup>. Importantly – at least for the combinations tested –  
293 severity was found to depend on the number but not identity of the *cox1* or *cob*  
294 introns present.

295

296 In addition to providing a new insight into post-transcriptional gene regulation in  
297 mitochondria, our findings have implications for understanding the evolutionary  
298 persistence of self-splicing introns and perhaps mobile elements more generally. The  
299 phenotypic effects we observe run counter to the notion that self-splicing introns are  
300 low-cost passengers and instead demonstrate that at least some of these selfish  
301 elements are firmly embedded in the organization of mitochondrial gene expression  
302 such that removing them upsets proper expression of their host genes. We suggest that  
303 our observations can be explained by an evolutionary lock-in model where the  
304 primordial colonization of an intron-free *cox1/cob* ancestor by a self-splicing intron  
305 led to a drop in *cox1/cob* mRNA levels and favoured compensatory mutations that  
306 increased *cox1/cob* transcription to restore mRNA abundances back to their original  
307 levels. When we forcibly remove these introns, however, this hard-wired upregulation  
308 turns maladaptive. There no longer is a pool of transcripts targeted for degradation  
309 leading to excess levels of mature mRNA. In principle, it is also possible that the  
310 initial invader spliced very efficiently and imposed no cost but subsequently co-  
311 evolved with host gene expression in a ratchet-like fashion, whereby incidental  
312 greater-than-required levels of the host gene allowed recurrent small decreases in  
313 splicing efficiency. However, since self-splicing introns can spread despite substantial  
314 fitness costs<sup>9</sup>, we do not actually need to evoke a cost-free ancestral event. We  
315 suggest that evolutionary lock-ins of this type might provide an unappreciated  
316 mechanism to facilitate the longer-term persistence of genetic parasites, especially in  
317 large host populations where evolution is not mutation-limited. We also note that this  
318 argument might in principle extend to nuclear introns: if, for a given dosage-sensitive  
319 gene, failure to splice is common and transcription levels are set to compensate, intron

320 loss might be deleterious and prevented by purifying selection even though the intron  
321 makes no adaptive contribution to gene regulation.

322

323

324

## 325 **Methods**

### 326 **Strains and growth conditions**

327 Strain a161 (also known as ID41-6/161, or sometimes simply 161), described by  
328 Wenzlau et al.<sup>23</sup>, and the intronless a161-U7 (*I<sub>0</sub>*) were gifts from Alan Lambowitz.  
329 These strains were used previously to show that splicing of group I and II introns is  
330 *Mss116*-dependent<sup>17</sup>. a161 and a161-U7 are isogenic except for the mitochondrial  
331 genome and a single marker gene (a161: MATa *ade1 lys1*; a161-U7: MATa *ade1 lys1*  
332 *ura3*).

333 Strain Y258 and the pBG1805 plasmid bearing *Mss116* for overexpression were  
334 purchased from Thermo Scientific (Dharmacon). *Mss116<sup>E268K</sup>* was purchased from  
335 DNA 2.0 and cloned into pBG1805 using standard cloning techniques<sup>24</sup>. *Mss116* and  
336 *Mss116<sup>E268K</sup>* were overexpressed in the Y258 nuclear background. The expression of  
337 *Mss116* and *Mss116<sup>E268K</sup>* was induced from the plasmids using 2% galactose (final),  
338 added at OD 0.2.

339 All strains were grown on YPD medium with 2% (w/v) glucose at 30°C with shaking.

340 All experiments were performed on exponentially growing cells: cells were grown to

341 OD 0.6-0.7 for WT, *I<sub>0</sub>*,  $\Delta$ Hap4, and  $\Delta$ Rtg2 and to OD 0.9-1.0 for *Mss116<sub>OE</sub>* and

342 *Mss116<sup>E268K</sup>*, harvested by centrifugation at 4000 × g for 5 minutes, washed and  
343 further treated as required.

344 In order to test growth on glycerol, strains were grown in YPD medium until  
345 saturation, at 30 °C with shaking. Stationary cells were serially diluted and 5 μL drops  
346 plated onto YPEG agar plates (containing 3% ethanol and 3% glycerol). Growth was  
347 observed after 4 days.

#### 348 **Gene deletion**

349 Deletion of *hap4* and *rtg2* was performed as previously described<sup>25</sup>, using a  
350 hygromycin cassette for selection in the WT background and a nourseothricine  
351 cassette in the *I<sub>0</sub>* background. Primers used for the deletions are listed in  
352 Supplementary File 1.

#### 353 **Measurement of splicing kinetics in *Mss116<sub>OE</sub>***

354 Overnight cultures of *Mss116<sub>OE</sub>* were diluted to OD 0.1. Galactose (2% final) was  
355 added at OD 0.2 to induce the expression of Mss116, and this is designated as time 0.  
356 Aliquots of the culture were harvested at 30, 60, 90, 120, 135, 150, 180, 210 and 240  
357 minutes post-induction. The cells were pelleted and used for RNA isolation and  
358 cDNA preparation for qPCR. Multiple primer pairs were used to monitor unspliced  
359 intron-exon fragments and spliced exon-exon junctions (Figure 2-figure supplement  
360 4, Supplementary File 1). Additional aliquots were harvested at 60, 150, 300, 360,  
361 420, and 540 minutes post-induction and were used to measure Mss116 expression  
362 levels by flow cytometry (see below).

363

## 364 **Insertion of point mutations into the promoter regions**

365 In order to introduce promoter-attenuating mutations into mitochondrial DNA, we  
366 followed the protocol described in<sup>26</sup> for the integration of altered mtDNA sequences  
367 by homologous double crossovers. Briefly, a mutant fragment of mtDNA (in this case  
368 promoter sequences) flanked by WT mtDNA sequence is first transformed into a *rho*<sup>0</sup>  
369 strain, which is then mated with a recipient *rho*<sup>+</sup> strain. Upon mating, mitochondria  
370 from the two strains fuse and recombination between the two mtDNAs produces  
371 recombinant *rho*<sup>+</sup> strains in which the new mtDNA sequence is integrated by double  
372 crossover. For transformation, tungsten powder was used as a carrier of DNA  
373 (Tungsten M-10 Microcarriers #1652266, BioRad). Bombardment was performed  
374 using the Biolistic PDS-1000/He particle delivery system (BioRad). Cells were  
375 transformed with linear DNA fragments obtained by ligation of each mutated  
376 promoter region with 500bp of up- and downstream flanking DNA (Supplementary  
377 File 1). SacI and Sall restriction sites were added by PCR for ligation between the 3'-  
378 end of the upstream flanking region and the 5'-end of the promoter sequence, and 3'-  
379 end of the promoter sequence and 5'-end of the downstream flanking region,  
380 respectively. The mutations introduced here (highlighted in Figure 5-figure  
381 supplement 1) have been previously shown to reduce the strength of *cox1* and *cob*  
382 promoters<sup>27</sup>.

383

## 384 **Chronological lifespan measurement**

385 All strains were grown to saturation as described above and pelleted at 4000 × g for  
386 5min. Cells were then washed twice and resuspended in sterile deionized water (10<sup>6</sup>

387 cells in 10mL in order to avoid cell growth on the debris of dead cells) and incubated  
388 at 30°C with shaking. Every 2-3 days, cells were serially diluted and plated onto YPD  
389 plates in order to evaluate cell growth.

390

### 391 **Replicative lifespan measurement**

392

393 Replicative lifespan (RLS) was determined by micromanipulation for *Mss116<sup>OE</sup>* and  
394 *Mss116<sup>E268K</sup>* in the Y258 background, as well as for *Mss116<sup>OE</sup>* in the  $\Delta hap4$  and  $\Delta rtg2$   
395 nuclear backgrounds, counting the number of daughters produced by individual  
396 mother cells. We were unable to reliably determine RLS for the *I<sub>0</sub>* strain as daughter  
397 and mother cells could not be separated in a timely manner, which is critical for RLS  
398 measurements. For unknown reasons, and perhaps specific to the nuclear background,  
399 cells were unusually sticky so that the first daughter often could not be separated from  
400 the mother until the mother had already produced other buds, making it difficult to  
401 track mother/daughter identity over time, an essential prerequisite for reliably  
402 determining replicative lifespan. Cells were incubated at 30°C on YPD (WT) or -  
403 URA (mutants) plates for the duration of the experiment. Using a microscope  
404 equipped with a microdissection apparatus suitable for *S. cerevisiae* (Singer  
405 Instruments), cells were transferred to defined places on agar plates and virgin  
406 daughter cells collected. Each cell was monitored continuously over several days  
407 every 60 - 90min until all mother cells stopped budding. The total number of daughter  
408 cells was noted for each mother cell. The total number of monitored mother cells is as  
409 follows: 90 cells for the empty vector control, 86 cells for *Mss116<sup>OE</sup>*, and 91 cells for  
410 the *Mss116<sup>E268K</sup>*. The measurements were pooled from 3 independent experiments.

411

## 412 **Respiration measurement**

413 Oxygen uptake was monitored polarographically using an oxygraph equipped with a  
414 Clark-type electrode (Oxygraph, Hansatech, Norfolk, UK). Cells were harvested  
415 during exponential growth phase, spun and resuspended in growth medium (as above)  
416 at the density of  $30 \times 10^6$  cells/mL. 500 $\mu$ L of culture were transferred to an airtight  
417 1.5mL oxygraph chamber. Cells were assayed in conditions closely similar to the  
418 ones in a flask culture (30°C and stirring). Oxygen content was monitored for at least  
419 4min. To ensure that the observed oxygen consumption was due to the mitochondrial  
420 activity, complex III inhibitor antimycin (final concentration 10 $\mu$ g/mL) was routinely  
421 added to the cultures and compared to the rate observed without antimycin.

422

## 423 **Competition assay**

424 Competition experiments were carried out between *I<sub>0</sub>* (a161-U7) and its control strain  
425 (a161) as well as between *MSS116OE* and its corresponding empty vector control  
426 strain. Prior to the competition, we plated  $5 \times 10^9$  cells of each mutant (*I<sub>0</sub>* or *MSS116OE*)  
427 strain on YPD agar plates with 200  $\mu$ g/mL geneticin, followed by a 4-day incubation  
428 at 30°C, to select for spontaneous geneticin resistance. In doing so, we can  
429 subsequently determine relative fitness in a relatively simple fashion using a plating  
430 method (rather than, for example, sequencing barcodes). The two strains to be  
431 competed were then grown independently on YPD medium in 2% glucose until  
432 saturation. The next day, an equal number of cells from each WT culture (geneticin-  
433 sensitive) and each mutant (geneticin-resistant) were mixed in fresh YPD medium,  
434 2% glucose so that each was diluted 200x. In mid-exponential phase, OD 0.4-0.6

435 (approximately 5-6 hours after dilution), aliquots of cells were harvested, and serial  
436 dilutions were plated on YPD-agar plates without geneticin. Next, dilutions with  
437 between 50 and 200 colonies were replica-plated on YPD-agar plates with geneticin  
438 (200  $\mu\text{g}/\text{mL}$ ). Colonies were counted on both types of plates and the ratio  
439 of geneticin-resistant (mutant) to geneticin-sensitive (WT) colonies was calculated as  
440 a measure of relative fitness.

441

#### 442 **Flow cytometry**

443 Flow cytometry was carried out on a Becton-Dickinson FACSCalibur machine  
444 equipped with a 488nm Argon laser and a 635nm red diode laser.

445

#### 446 **Measurement of the Mss116 overexpression level**

447 The expression level of Mss116 in the *MSS116<sub>OE</sub>* strain was measured by using a  
448 rabbit polyclonal anti-His tag antibody (Abcam, ab137839, 1:10000) and secondary  
449 IgG goat anti-rabbit labeled with Alexa 488 (Thermo Fisher Scientific, A11034,  
450 1:2000). The signal obtained by flow cytometry (mean fluorescence over 10000 cells)  
451 was compared to the Mss116 tagged with GFP (Thermo Scientific) endogenous  
452 expression level estimated by using flow cytometry measurement based on the GFP  
453 signal. The mean fluorescence intensity in *MSS116<sub>OE</sub>* was normalized to the mean  
454 fluorescence intensity detected in wild type cells with endogenous expression of  
455 Mss116.

#### 456 **Mass spectrometry - sample processing**

457 Isolated mitochondrial fractions containing 100µg of protein were loaded onto  
458 Microcon 30kD centrifugal filters (Merck Millipore, MRCF0R030). Samples were  
459 then digested using a Filter Aided Sample Preparation (FASP) protocol<sup>28</sup>. Briefly,  
460 samples were concentrated on the filter unit by centrifugation and buffer exchanged  
461 using sequential washing and centrifugation with 8M urea, 100mM TRIS/HCL buffer  
462 (pH8.5). Proteins were reduced and alkylated sequentially with 10mM Dithiothreitol  
463 and 50mM Iodoacetamide (in 8M urea buffer), respectively. Samples were buffer  
464 exchanged to remove salts using sequential washing with 50mM ammonium  
465 bicarbonate (AmBic). Trypsin Gold (Promega, V5280) was added to the samples in  
466 50mM ammonium bicarbonate to an approximate 1:50, protease:protein ratio.  
467 Digestions were incubated at 37°C overnight (17h). Digest extracts were recovered  
468 from FASP filters via centrifugation and acidified with 1% trifluoroacetic acid (TFA).  
469 Acidified protein digests were desalted using Glygen C18 spin tips (Glygen Corp,  
470 TT2C18.96) according to the manufacturer's recommendation and peptides eluted  
471 with 60% acetonitrile, 0.1% formic acid (FA). Eluents were then dried using a  
472 vacuum centrifuge.

473

474 **Mass spectrometry - liquid chromatography-tandem mass spectrometry (LC-**  
475 **MS/MS) analysis**

476

477 Protein digests were redissolved in 0.1% TFA by shaking (1200rpm) for 30min and  
478 sonication on an ultrasonic water bath for 10min, followed by centrifugation  
479 (14,000rpm, 5°C) for 10min. LC-MS/MS analysis was carried out in technical  
480 duplicates (1µg on column) and separation was performed using an Ultimate 3000  
481 RSLC nano liquid chromatography system (Thermo Scientific) coupled to a Orbitrap

482 Velos mass spectrometer (Thermo Scientific) via an Easy-Spray source. For LC-  
483 MS/MS analysis protein digests were injected and loaded onto a trap column  
484 (Acclaim PepMap 100 C18, 100 $\mu$ m  $\times$  2cm) for desalting and concentration at  
485 8 $\mu$ L/min in 2% acetonitrile, 0.1% TFA. Peptides were then eluted on-line to an  
486 analytical column (Easy-Spray Pepmap RSLC C18, 75 $\mu$ m  $\times$  50cm) at a flow rate of  
487 250nL/min. Peptides were separated using a 120 minute gradient, 4-25% of buffer B  
488 for 90 minutes followed by 25-45% buffer B for another 30 minutes (composition of  
489 buffer B – 80% acetonitrile, 0.1% FA) and subsequent column conditioning and  
490 equilibration. Eluted peptides were analysed by the mass spectrometer operating in  
491 positive polarity using a data-dependent acquisition mode. Ions for fragmentation  
492 were determined from an initial MS1 survey scan at 30,000 resolution, followed by  
493 CID (Collision Induced Dissociation) of the top 10 most abundant ions. MS1 and  
494 MS2 scan AGC targets were set to 1e6 and 3e4 for maximum injection times of  
495 500ms and 100ms respectively. A survey scan m/z range of 350 – 1500 was used,  
496 normalised collision energy set to 35%, charge state screening enabled with +1 charge  
497 states rejected and minimal fragmentation trigger signal threshold of 500 counts.

498

#### 499 **Mass spectrometry - raw data processing**

500

501 Data was processed using the MaxQuant software platform (v1.5.6.0), with database  
502 searches carried out by the in-built Andromeda search engine against the Uniprot  
503 *S.cerevisiae* database (version 20160815, number of entries: 6,729). A reverse decoy  
504 database approach was used at a 1% false discovery rate (FDR) for peptide spectrum  
505 matches. Search parameters included: maximum missed cleavages set to 2, fixed  
506 modification of cysteine carbamidomethylation and variable modifications of

507 methionine oxidation, asparagine deamidation and N-terminal glutamine to  
508 pyroglutamate conversion. Label-free quantification was enabled with an LFQ  
509 minimum ratio count of 2. ‘Match between runs’ function was used with match and  
510 alignment time limits of 1 and 20 minutes respectively. Data have been deposited in  
511 the PRIDE repository [project accession number PXD008785].

512

### 513 **Assessment of mitochondrial membrane potential and mass**

514 Variations of the mitochondrial transmembrane potential ( $\Delta\Psi_m$ ) were studied using  
515 3,3-dihexyloxacarbocyanine iodide [DiOC6(3)]. This cyanine cationic dye  
516 accumulates in the mitochondrial matrix as a function of  $\Delta\Psi_m$ <sup>29</sup>. Cells ( $1 \times 10^6$ /mL)  
517 were incubated in 1mL culture medium containing 40nM DiOC6(3) for 30min in the  
518 dark at 30°C with constant shaking. DiOC6(3) membrane potential-related  
519 fluorescence was recorded using FL1 height. A total of 10,000 cells were analyzed for  
520 each curve. The collected data was analyzed using FlowJo software version 7.2.5 to  
521 determine the mean green fluorescence intensity after each treatment. The results are  
522 expressed as a percentage of mean fluorescence of the control strain. As a negative  
523 control, in each experiment, we preincubated aliquots of cells with carbonyl-cyanide  
524 4-(trifluoromethoxy)- phenylhydrazone (FCCP, Sigma) and antimycin (Sigma) at  
525 100 $\mu$ M and 5 $\mu$ g/mL, respectively, 10min before fluorescent dye staining, which leads  
526 to a collapse of mitochondrial membrane potential.

527 To measure mitochondrial mass, we used 10-N-Nonyl acridine orange (NAO), a dye  
528 that binds to cardiolipin, a phospholipid specifically present on the mitochondrial  
529 membrane<sup>29</sup>. Cells ( $1 \times 10^6$ /mL) were incubated in 1 mL culture medium containing  
530 100nM NAO for 30min in the dark at 30°C with constant shaking, followed by

531 analysis on FACSCalibur flow cytometer with the same photomultiplier settings as  
532 used for DiOC6(3).

533

#### 534 **Evaluation of the mitochondrial morphology and protein import machinery**

535 To image mitochondrial morphology, strains were transformed with a MitoLoc  
536 plasmid<sup>30</sup> (a gift from Markus Ralser) according to a previously described protocol<sup>31</sup>,  
537 with the only difference that the cells were incubated with the plasmid overnight at  
538 room temperature. Microscope slides were prepared as follows: 150 $\mu$ L of YPD media  
539 containing 2% agarose was placed on a preheated microscope slide and cooled, before  
540 applying yeast cells to obtain a monolayer. The cells were centrifuged at 4000  $\times$  g for  
541 3min, and resuspended in 50 $\mu$ L YPD. Once dry, the cover slip was placed, sealed, and  
542 mounted on a temperature-controlled Nikon Ti-E Eclipse inverted/UltraVIEW VoX  
543 (Perkin Elmer) spinning disc confocal setup, driven by Volocity software (version  
544 6.3; Perkin Elmer). Images were recorded through a 60xCFI PlanApo VC oil  
545 objective (NA 1.4) using coherent solid state 488nm and 543nm diode lasers with a  
546 DPSS module, and a 1000  $\times$  1000 pixel 14-bit Hamamatsu (C9100-50) electron-  
547 multiplied, charge-coupled device (EMCCD). The exposure time was 100ms for GFP  
548 and 300ms for mCherry, at 5–10% laser intensity. The number of cells with cytosolic  
549 mCherry accumulation was counted manually. More than 1000 cells were examined  
550 for each strain. Images were analysed using ImageJ software with the MitoLoc  
551 plugin.

552

#### 553 **ROS measurement**

554 Cells were incubated in the dark with 5 $\mu$ M MitoSOX<sup>TM</sup> red mitochondrial superoxide  
555 indicator (Molecular Probes) for 10min at 30°C and subsequently analyzed by flow  
556 cytometry. Fluorescence (excitation/emission maxima of 510/580nm) of 10,000 cells  
557 resulting from the intracellular red fluorescence was measured in the FL2 channel.  
558 The collected data was analyzed using FlowJo software version 7.2.5 for Microsoft  
559 (TreeStar, San Carlos, CA, USA) to determine the mean green fluorescence intensity  
560 after each treatment. The results are expressed as the mean fluorescence across 10,000  
561 cells.

562

### 563 **RNA extraction**

564 Total RNA was isolated using the NucleoSpin RNA kit (Macherey&Nagel) according  
565 to the manufacturer's instructions for up to 3  $\times$  10<sup>8</sup> yeast cells, which includes  
566 incubation with 50–100U of zymolyase for 1hr at 30°C. The quality of the resulting  
567 total RNA was tested on 1% agarose gels.

568

### 569 **Genomic DNA isolation**

570 Cells from saturated cultures (approximately 10<sup>9</sup> cells) of WT Y258, WT a161, *I<sub>0</sub>*,  
571 and *Mss116<sup>OE</sup>* were harvested by centrifugation and washed, as described above. Cell  
572 wall was digested for 1h at 30°C in the presence of 50–100U of zymolyase.  
573 Spheroplasts were then resuspended in 500 $\mu$ L of cell lysis buffer (75mM NaCl,  
574 50mM EDTA, 20mM HEPES pH 7.8, 0.2% SDS). Next, 10 $\mu$ L of 20mg/mL  
575 proteinase K was added and the mixture incubated for 2h at 50°C. DNA was

576 precipitated by the addition of isopropanol at room temperature, followed by  
577 centrifugation at 4°C and 11000g for 30min. The DNA pellet was then washed with  
578 ice-cold 70% ethanol, air-dried and resuspended in 50µL of DNase free water at  
579 55°C.

580

### 581 **Quantitative real-time PCR (qPCR)**

582 cDNA was synthesized from 1000ng of total RNA using the iScript™ cDNA  
583 Synthesis Kit (Biorad). The cDNA was diluted 100-fold, mixed with primer pairs for  
584 each gene and SYBRgreen (BioRad). All primer pairs were designed to have a  
585 melting temperature of 60°C and are listed in Supplementary File 1. The qPCR  
586 reaction was run on a QuantFlexStudio 6 (Life Technologies) using 40 cycles, after  
587 which the melting curves for each well were determined. Final fold change values  
588 were estimated relative to the UBC6 gene in the control strain replicates.

589 mtDNA copy number was assessed by qPCR using genomic DNA as template and  
590 primers against *cox1* and *cox3* (mtDNA) and *rpl32* (nuclear DNA, for normalization).

591

### 592 **Single cell generation time measurement**

593 Individual cells (approximately 100 for each strain) were placed on agar plates of  
594 appropriate growth medium, as described above, using a micromanipulator. Next, an  
595 image of each original mother cell was taken every 10 minutes for 8-9 hours. The  
596 images were then analysed and division time of each cell was extracted.

597

598

599

### 600 **RNA-FISH and imaging**

601

602 Yeast cultures were grown as described above, fixed with 37% formaldehyde for  
603 45min at room temperature, digested with 2.5 $\mu$ L of zymolyase (Zymo Research,  
604 2000 U) at 30°C for 60min and permeabilized with 70% ethanol overnight at 4°C.  
605 Cells were hybridized in the dark at 30°C using Stellaris RNA-FISH probes  
606 (Biosearch Technologies). 45 probes targeting intron aI2 and 40 probes targeting  
607 intron aI5b *coxI* were coupled to Quasar 670 dye (red). 43 probes targeting *coxI*  
608 exons were coupled to Quasar 570 dye (green). Yeast cells were placed on  
609 microscope slides with Vectashield Mounting Medium and imaged with an Olympus  
610 IX70 wide-field fluorescence microscope. A series of z-stacks was acquired with a  
611 step size of 0.3 $\mu$ m. The images were analysed using Image J. The number of green  
612 (exon), red (intron) and yellow (colocalized) foci was manually counted and  
613 normalized per 100 cells in each of three biological replicates. At least 300 cells were  
614 analyzed per replicate per strain.

615

### 616 **References**

617

- 618 1. Werren, J. H. Selfish genetic elements, genetic conflict, and evolutionary  
619 innovation. *Proceedings of the National Academy of Sciences of the United*  
620 *States of America* **108 Suppl 2**, 10863–10870 (2011).
- 621 2. Hurst, G. D. D. & Werren, J. H. The role of selfish genetic elements in  
622 eukaryotic evolution. *Nat. Rev. Genet.* **2**, 597–606 (2001).
- 623 3. Feschotte, C. Transposable elements and the evolution of regulatory networks.

- 624 *Nat. Rev. Genet.* **9**, 397–405 (2008).
- 625 4. Lambowitz, A. M. & Belfort, M. Introns as Mobile Genetic Elements. *Annu.*  
626 *Rev. Biochem.* **62**, 587–622 (1993).
- 627 5. Goddard, M. R. & Burt, A. Recurrent invasion and extinction of a selfish gene.  
628 *Proceedings of the National Academy of Sciences of the United States of*  
629 *America* **96**, 13880–13885 (1999).
- 630 6. Skelly, P. J. & Maleszka, R. Distribution of mitochondrial intron sequences  
631 among 21 yeast species. *Curr Genet* **19**, 89–94 (1991).
- 632 7. Dujon, B. Group I introns as mobile genetic elements: Facts and mechanistic  
633 speculations — a review. *Gene* **82**, 91–114 (1989).
- 634 8. Repar, J. & Warnecke, T. Mobile Introns Shape the Genetic Diversity of Their  
635 Host Genes. *Genetics* **205**, 1641–1648 (2017).
- 636 9. Hickey, D. A. Selfish DNA: a sexually-transmitted nuclear parasite. *Genetics*  
637 **101**, 519–531 (1982).
- 638 10. Séraphin, B., Boulet, A., Simon, M. & Faye, G. Construction of a yeast strain  
639 devoid of mitochondrial introns and its use to screen nuclear genes involved in  
640 mitochondrial splicing. *Proceedings of the National Academy of Sciences of the*  
641 *United States of America* **84**, 6810–6814 (1987).
- 642 11. Minczuk, M., Dmochowska, A., Palczewska, M. & Stepień, P. P.  
643 Overexpressed yeast mitochondrial putative RNA helicase Mss116 partially  
644 restores proper mtRNA metabolism in strains lacking the Suv3 mtRNA  
645 helicase. *Yeast* **19**, 1285–1293 (2002).
- 646 12. Paumard, P. *et al.* The ATP synthase is involved in generating mitochondrial  
647 cristae morphology. *The EMBO Journal* **21**, 221–230 (2002).
- 648 13. Velours, J., Dautant, A., Salin, B., Sagot, I. & Brèthes, D. Mitochondrial F1F0-

- 649 ATP synthase and organellar internal architecture. *The International Journal of*  
650 *Biochemistry & Cell Biology* **41**, 1783–1789 (2009).
- 651 14. Wolters, J. F., Chiu, K. & Fiumera, H. L. Population structure of mitochondrial  
652 genomes in *Saccharomyces cerevisiae*. *BMC Genomics* **16**, 281 (2015).
- 653 15. Dujon, B. Sequence of the intron and flanking exons of the mitochondrial 21S  
654 rRNA gene of yeast strains having different alleles at the omega and rib-1 loci.  
655 *Cell* **20**, 185–197 (1980).
- 656 16. Karunatilaka, K. S., Solem, A., Pyle, A. M. & Rueda, D. Single-molecule  
657 analysis of Mss116-mediated group II intron folding. *Nature* **467**, 935–939  
658 (2010).
- 659 17. Huang, H.-R. *et al.* The splicing of yeast mitochondrial group I and group II  
660 introns requires a DEAD-box protein with RNA chaperone function.  
661 *Proceedings of the National Academy of Sciences of the United States of*  
662 *America* **102**, 163–168 (2005).
- 663 18. Markov, D. A., Wojtas, I. D., Tessitore, K., Henderson, S. & McAllister, W. T.  
664 Yeast DEAD box protein Mss116p is a transcription elongation factor that  
665 modulates the activity of mitochondrial RNA polymerase. *Molecular and*  
666 *Cellular Biology* **34**, 2360–2369 (2014).
- 667 19. Munding, E. M., Shiue, L., Katzman, S., Donohue, J. P. & Ares, M.  
668 Competition between pre-mRNAs for the splicing machinery drives global  
669 regulation of splicing. *Molecular Cell* **51**, 338–348 (2013).
- 670 20. Wang, G.-S. & Cooper, T. A. Splicing in disease: disruption of the splicing  
671 code and the decoding machinery. *Nat. Rev. Genet.* **8**, 749–761 (2007).
- 672 21. Heintz, C. *et al.* Splicing factor 1 modulates dietary restriction and TORC1  
673 pathway longevity in *C. elegans*. *Nature* **541**, 102–106 (2017).

- 674 22. Golik, P., Szczepanek, T., Bartnik, E., Stepien, P. P. & Lazowska, J. The S.  
675 cerevisiae nuclear gene SUV3 encoding a putative RNA helicase is necessary  
676 for the stability of mitochondrial transcripts containing multiple introns. *Curr*  
677 *Genet* **28**, 217–224 (1995).
- 678 23. Wenzlau, J. M., Saldanha, R. J., Butow, R. A. & Perlman, P. S. A latent intron-  
679 encoded maturase is also an endonuclease needed for intron mobility. *Cell* **56**,  
680 421–430 (1989).
- 681 24. Sambrook, J. & Maniatis, T. *Molecular Cloning*. (Cold Spring Harbor  
682 Laboratory Press, 1989).
- 683 25. Rothstein, R. J. One-step gene disruption in yeast. *Meth. Enzymol.* **101**, 202–  
684 211 (1983).
- 685 26. Bonnefoy, N., Remacle, C. & Fox, T. D. in *Mitochondria, 2nd Edition* **80**,  
686 525–548 (Elsevier, 2007).
- 687 27. Turk, E. M., Das, V., Seibert, R. D. & Andrulis, E. D. The Mitochondrial RNA  
688 Landscape of *Saccharomyces cerevisiae*. *PLoS ONE* **8**, e78105 (2013).
- 689 28. Wiśniewski, J. R., Zougman, A., Nagaraj, N. & Mann, M. Universal sample  
690 preparation method for proteome analysis. *Nat Meth* **6**, 359–362 (2009).
- 691 29. Perry, S., Norman, J., Barbieri, J., Brown, E. & Gelbard, H. Mitochondrial  
692 membrane potential probes and the proton gradient: a practical usage guide.  
693 *BioTechniques* **50**, 98–115 (2011).
- 694 30. Vowinckel, J., Hartl, J., Butler, R. & Ralser, M. MitoLoc: A method for the  
695 simultaneous quantification of mitochondrial network morphology and  
696 membrane potential in single cells. *Mitochondrion* **24**, 77–86 (2015).
- 697 31. Gietz, R. D. & Schiestl, R. H. High-efficiency yeast transformation using the  
698 LiAc/SS carrier DNA/PEG method. *Nat Protoc* **2**, 31–34 (2007).

699

700

701

702 **Acknowledgements**

703 The authors would like to thank Tea Copic, Martin Billman, Sam Marguerat, and Xi  
704 Ming Sun for experimental assistance, Holger Kramer and the LMS Proteomics  
705 facility for proteomics work, and Nuno Raimundo, Ira Milosevic, Santiago Vernia,  
706 and Laurence Hurst for discussions. This work was supported by funding from the  
707 NAOS Group and the Mediterranean Institute for Life Sciences (MR, MM, MK, AK),  
708 an Imperial College Junior Research Fellowship (TW) and UK Medical Research  
709 Council core funding (TW).

710

711 **Competing financial interests**

712 The authors declare that no competing financial interests exist.

713

714

715

716

717 **Figure legends**

718

719 **Figure 1. Phenotypic effects of deleting all self-splicing introns from the *S.***  
720 ***cerevisiae* mitochondrial genome.**

721 Deletion of mitochondrial introns (*I<sub>0</sub>*) or overexpression of Mss116 (*MSS116<sup>OE</sup>*) (a)  
722 reduces growth rates, (b) extends chronological lifespan, (c) increases mitochondrial  
723 mass, measured as NAO fluorescence, (d,e) increases mitochondrial volume, (g)

724 oxygen consumption, and (h) ATP levels but (i) decreases superoxide levels,  
725 measured as MitoSOX fluorescence. (f) Mitochondrial inner membrane potential does  
726 not differ significantly between strains. WT a161 and WT Y258 are control strains for  
727 *I<sub>0</sub>* and *Mss116<sub>OE</sub>*, respectively, as described in the text. The *Mss116<sup>E268K</sup>* strain  
728 harbours a mutant version of Mss116 that lacks ATPase activity. As a visual guide,  
729 strains are coloured consistently throughout. Bar heights display the mean of three  
730 biological replicates, each calculated as the mean of three technical replicates. Error  
731 bars are standard errors of the mean. \*\*\*P < 0.001; \*\*P < 0.01; \*P < 0.05 (ANOVA  
732 plus post hoc).

733

734 **Figure 2. RNA abundance changes associated with intron removal.**

735 (a) qPCR measurements of selected genes, comparing focal strains (*I<sub>0</sub>*, *Mss116<sub>OE</sub>*,  
736 *Mss116<sup>E268K</sup>*) to their isogenic control strains (left panel). For both *cox1* (central  
737 panel) and *cob* (right panel), intron levels are specifically reduced upon  
738 overexpression of *Mss116<sub>OE</sub>* but not *Mss116<sup>E268K</sup>*, while mature mRNA levels  
739 increase. Heat maps display mean values of log-fold changes observed across three  
740 biological replicates (each averaged over three technical replicates). UBC6 was used  
741 for normalization.

742 (b) RNA-FISH confirms elimination/reduction of introns aI2 and aI5 $\beta$  from the *cox1*  
743 transcript pool. Exon (green), intron (red) and co-localized (green/red) puncta were  
744 counted in more than 300 cells. The bar chart shows the number of signals per 100  
745 cells. Bar heights display the mean of three biological replicates (each averaged over  
746 three technical replicates). Error bars are standard error of the mean. \*\*\*P < 0.001;  
747 \*\*P < 0.01; \*P < 0.05 (ANOVA plus post hoc). White lines mark cell boundaries.

748 White arrows mark examples of exonic puncta that do not co-localize with intronic  
749 puncta.

750 (c) qPCR time series of pre-mRNA and mature mRNA levels following induction of  
751 *Mss116*. Mature mRNA for *cox1* and *cob* was quantified using primer pairs ( $f_{xT}$ ,  $f_{bT}$ )  
752 overlapping the terminal exon-exon junctions. Pre-mRNA was quantified using a  
753 series of primer pairs ( $f_{x1-5}$ ,  $f_{b1-5}$ ). For each pair, one primer is located in exonic, the  
754 other in intronic sequence, as detailed in Figure 2-figure supplement 4. Each circle  
755 (shades of blue for the pre-mRNA and red for the mature transcript) represents the  
756 mean value from three biological replicates (each averaged over three technical  
757 replicates). UBC6 was used for normalization.

758

759 **Figure 3. The intronless phenotype requires a functional retrograde response.**

760 (a) Mitochondrial morphology is altered and (b) mitochondrial volume, (c) oxygen  
761 consumption, (d) ATP levels, and (e) chronological lifespan are reduced when *rtg2* is  
762 deleted in the *I<sub>0</sub>* or *MSS116<sup>OE</sup>* background. This contrasts sharply with *I<sub>0</sub>* and  
763 *MSS116<sup>OE</sup>* where *rtg2* is intact (see Figure 1). Bar heights display the mean of three  
764 biological replicates (each averaged over three technical replicates). Error bars are  
765 standard error of the mean. \*\*\*P < 0.001; \*\*P < 0.01; \*P < 0.05 (ANOVA plus post  
766 hoc). (f) Transcriptional responses in different strains where *rtg2* has been deleted, as  
767 measured by qPCR. Heat maps display mean values of log-fold changes observed  
768 across three biological replicates (each averaged over three technical replicates).  
769 UBC6 was used for normalization.

770

771 **Figure 4. Hap4 is required for the intronless phenotype.**

772 (a) Mitochondrial morphology, (b) mitochondrial volume, (c) oxygen consumption,  
773 (d) ATP levels, and (e) chronological lifespan do not differ between *I0/Mss116OE* and  
774 their corresponding control strains if *hap4* has been deleted. Bar heights display the  
775 mean of three biological replicates (each averaged over three technical replicates).  
776 Error bars are standard error of the mean. \*\*\*P < 0.001; \*\*P < 0.01; \*P < 0.05  
777 (ANOVA plus post hoc). (f) Transcriptional responses in different strains where *hap4*  
778 has been deleted, as measured by qPCR. Heat maps display mean values of log-fold  
779 changes observed across three biological replicates (each averaged over three  
780 technical replicates). UBC6 was used for normalization.

781

782 **Figure 5. Dampening RNA levels of *cox1* and *cob* by reducing promoter activity**  
783 **partially rescues the intronless phenotype.**

784 (a) qPCR measurements in strains where either the *cob* promoter (*cobp*), the *cox1*  
785 promoter (*cox1p*) or both (*pp*) have been attenuated via targeted mutations. Heat maps  
786 display mean values of log-fold changes observed across three biological replicates  
787 (each averaged over three technical replicates). UBC6 was used for normalization.

788 (b) Oxygen consumption and (c) mitochondrial morphology and (d) volume in  
789 response to promoter attenuation. Bar heights display the mean of three biological  
790 replicates (each averaged over three technical replicates). Error bars are standard error  
791 of the mean. Asterisks to indicate statistical significance are omitted for clarity. All  
792 comparisons between single- and double-promoter mutants and the corresponding  
793 parent strains are significant at P<0.001 (ANOVA plus post hoc).

794

795

796 **Supplementary Figure Legends**

797

798 **Figure 1-figure supplement 1.** Competitive fitness is decreased in *I<sub>0</sub>* (competed  
799 against WT a161) and *MSS116<sub>OE</sub>* (competed against the empty vector control WT  
800 Y258). Bar height represents the mean of three biological replicates. Error bars are  
801 standard error of the mean. \*\*\*P < 0.001; \*\*P < 0.01; \*P < 0.05 (ANOVA plus post  
802 hoc). See Methods for details of how competitions were carried out and relative  
803 fitness determined.

804

805 **Figure 1-figure supplement 2.** *I<sub>0</sub>* and *MSS116<sub>OE</sub>* show no qualitative difference in  
806 growth on (a) glucose and (b) glycerol. Numbers on top of each panel represent the  
807 decimal dilution of the stationary culture that is plated as a spot of 5  $\mu$ l.

808

809 **Figure 1-figure supplement 3.** (a) GFP-tagged Mss116 localizes to mitochondria,  
810 whether expressed at endogenous levels (left image) or upon overexpression in the  
811 Y258 background (right image). (b) The expression level of Mss116 increases  
812 approximately 2.5-fold in the *MSS116<sub>OE</sub>* strain, as measured by flow cytometry. Bar  
813 heights display the mean of three biological replicates, each of them representing  
814 mean of three technical replicates. Error bars are standard error of the mean. \*\*\*P <  
815 0.001; \*\*P < 0.01; \*P < 0.05 (ANOVA plus post hoc).

816

817 **Figure 1-figure supplement 4.** Median and maximum replicative lifespan of  
818 *MSS116<sub>OE</sub>* is extended compared to the empty vector control and *MSS116<sup>E268K</sup>*. The  
819 total number of monitored mother cells is as follows: 90 cells for the empty vector  
820 control, 86 cells for *MSS116<sub>OE</sub>*, and 91 cells for the *MSS116<sup>E268K</sup>*. Measurements were  
821 pooled across 3 independent experiments.

822

823 **Figure 2-figure supplement 1.** (a) Comparison of qPCR measurements in *I<sub>0</sub>* and *I<sub>0</sub>*  
824 overexpressing *Mss116*. Heat maps display mean values of log-fold changes observed  
825 across three biological replicates (each averaged over three technical replicates).  
826 *UBC6* was used for normalization. (b) ATP level, (c) oxygen consumption and (d)  
827 ROS level do not change upon overexpression of *Mss116* in the *I<sub>0</sub>* genetic background  
828 (*I<sub>0</sub>* + *Mss116<sup>OE</sup>*) compared to *I<sub>0</sub>*.

829

830 **Figure 2-figure supplement 2.** *Mss116* deletion does not affect *I<sub>0</sub>* phenotypes,  
831 highlighted by (a) the transcript levels (measured by qPCR) of relevant genes, (b)  
832 mitochondrial morphology, and (c) mitochondrial volume. The heat map displays  
833 mean values of log-fold changes observed across three biological replicates (each  
834 averaged over three technical replicates). *UBC6* was used for normalization. In panel  
835 (c), bar heights display the mean of three biological replicates (each averaged over  
836 three technical replicates). Error bars are standard error of the mean. \*\*\*P < 0.001;  
837 \*\*P < 0.01; \*P < 0.05 (ANOVA plus post hoc).

838

839 **Figure 2-figure supplement 3.** Expression level of *Mss116* during 9 hours after  
840 induction using 2% galactose. Circles represent mean value of three biological  
841 replicates (each performed as technical replicate). Error bars are standard error of the  
842 mean.

843

844 **Figure 2-figure supplement 4.** Schematic presentation of the fragments of *cox1* and  
845 *cob* amplified to determine the pre-mRNA and mature mRNA levels.

846

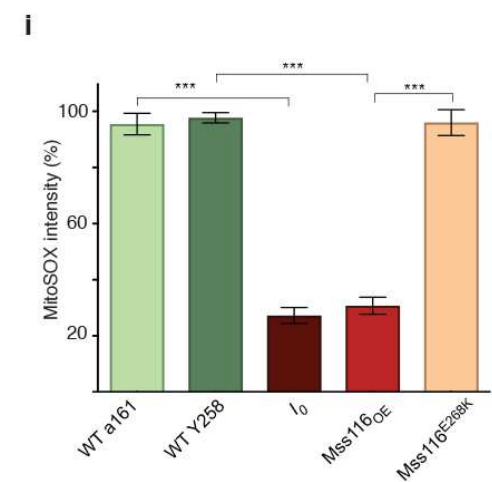
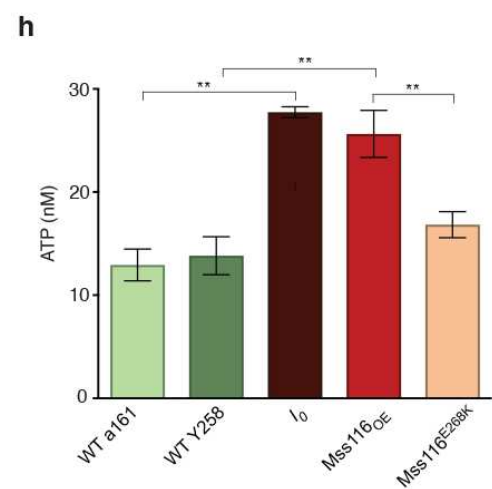
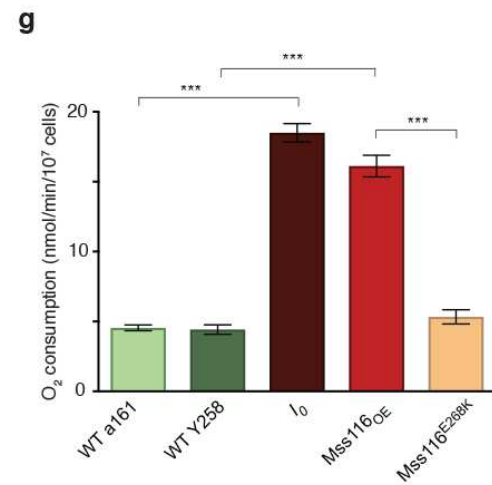
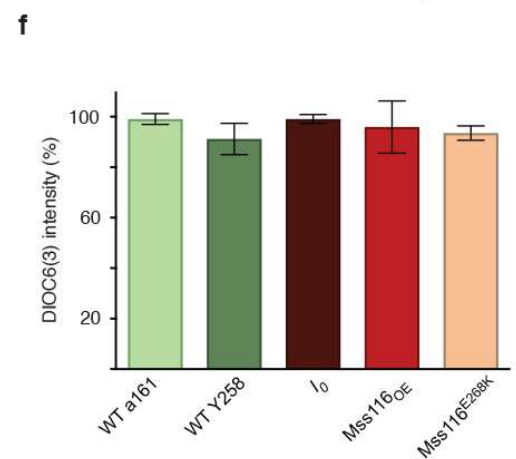
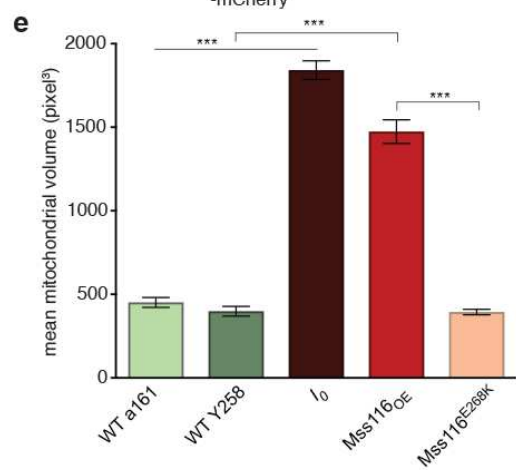
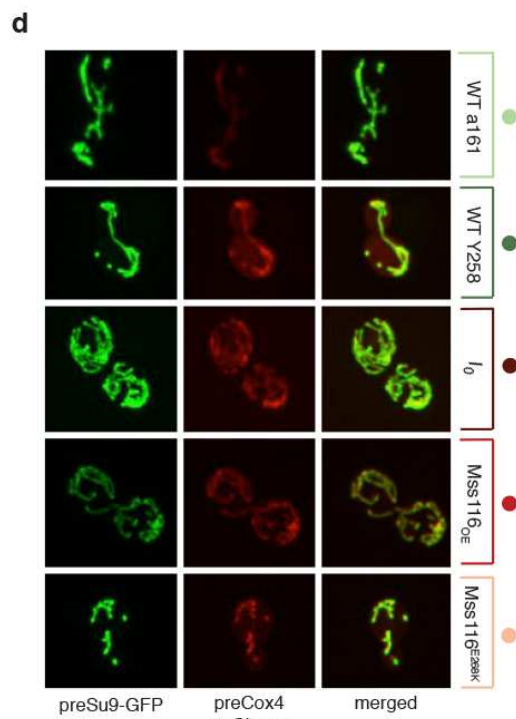
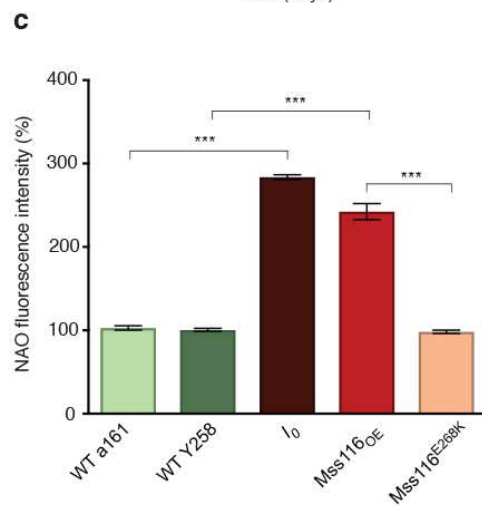
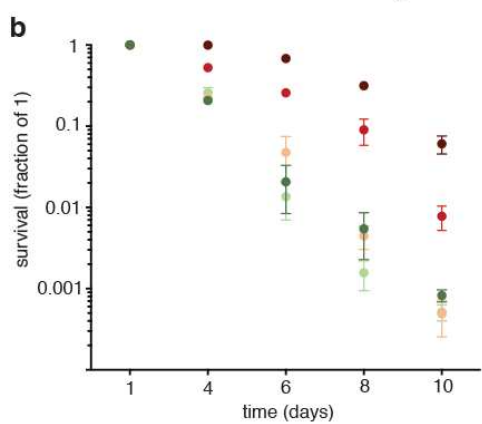
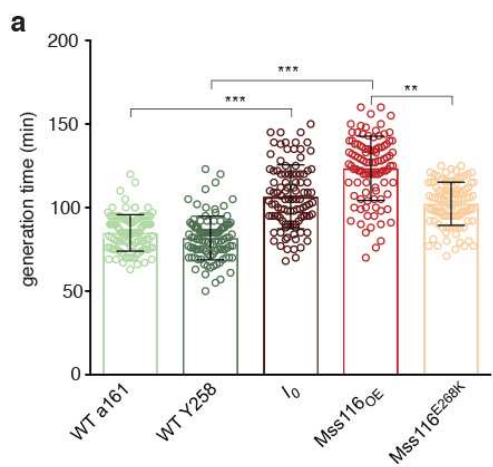
847 **Figure 5-figure supplement 1.** *Related to Figure 5.* Schematic representation of  
848 mutated positions in the promoter regions of *cox1* and *cob*.

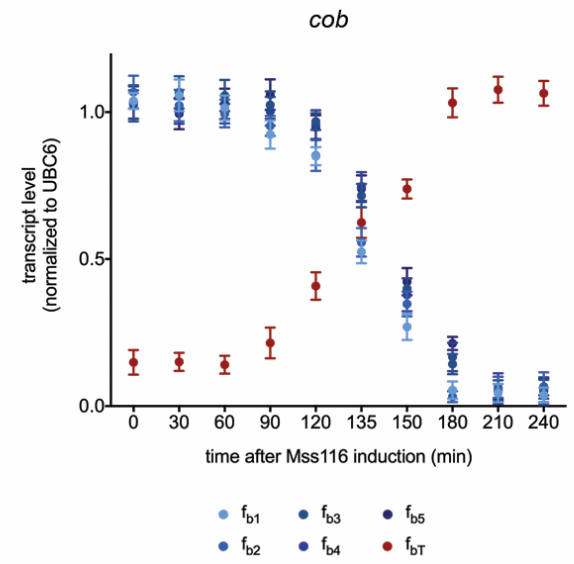
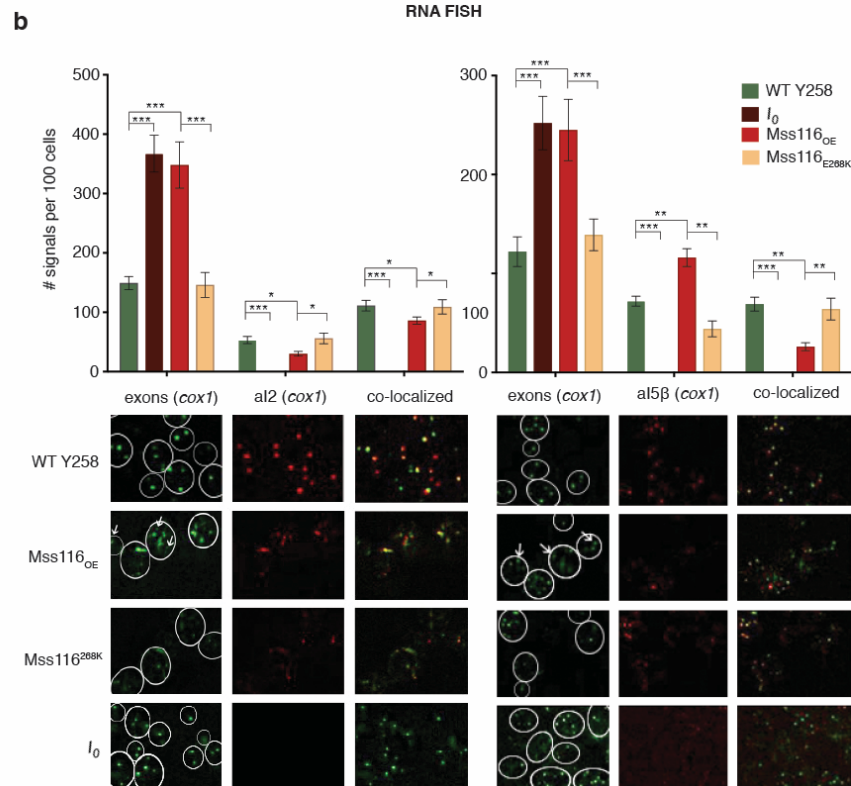
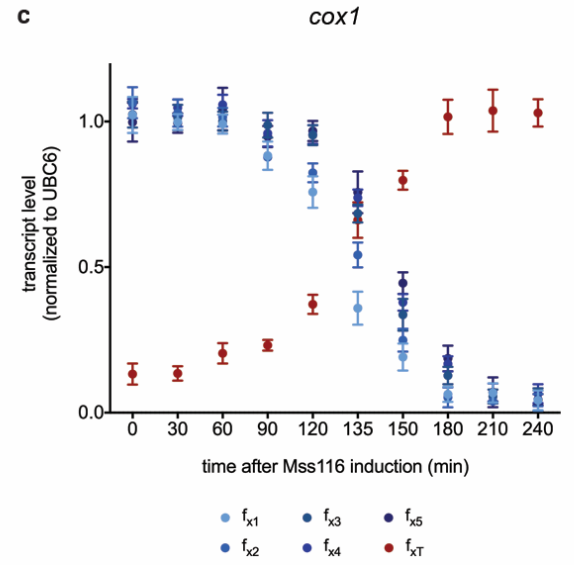
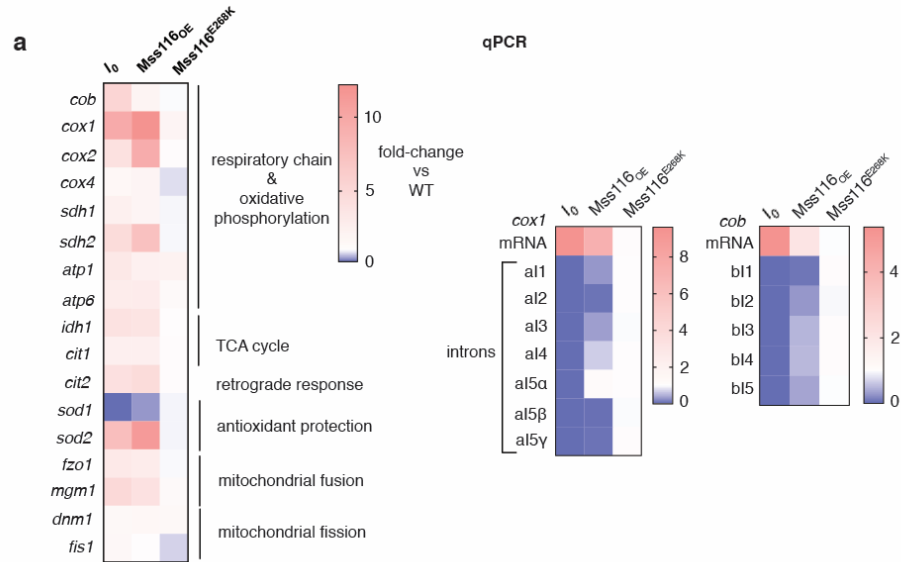
849

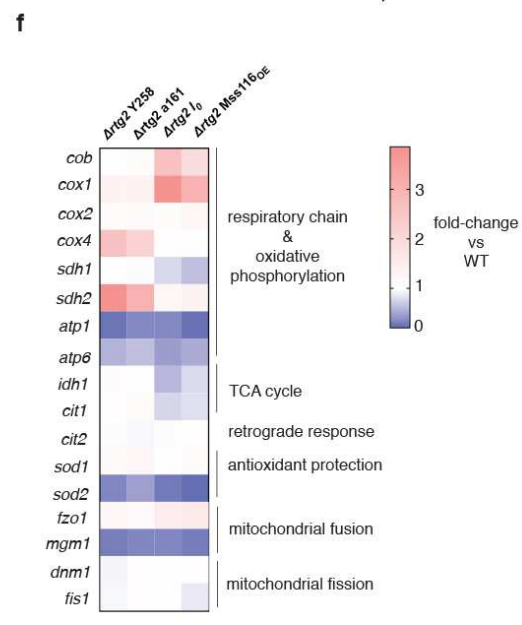
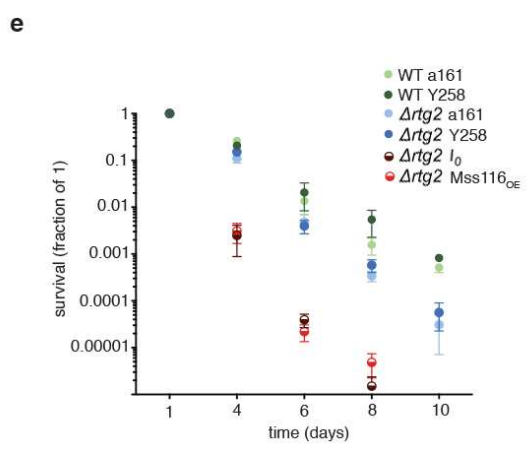
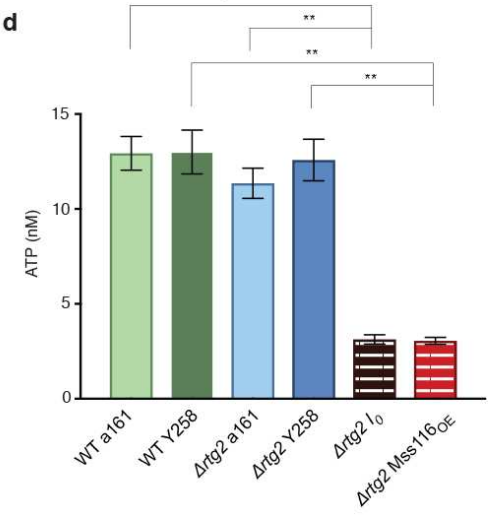
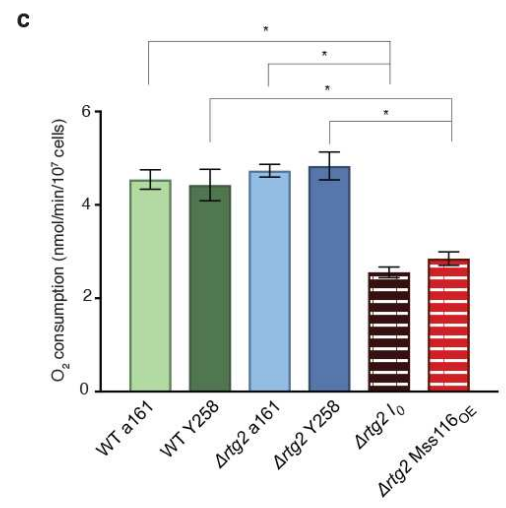
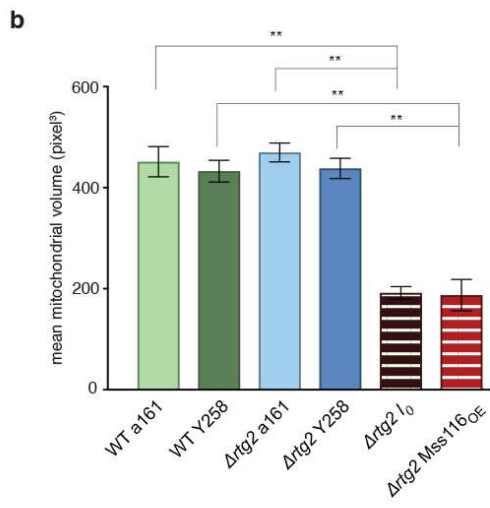
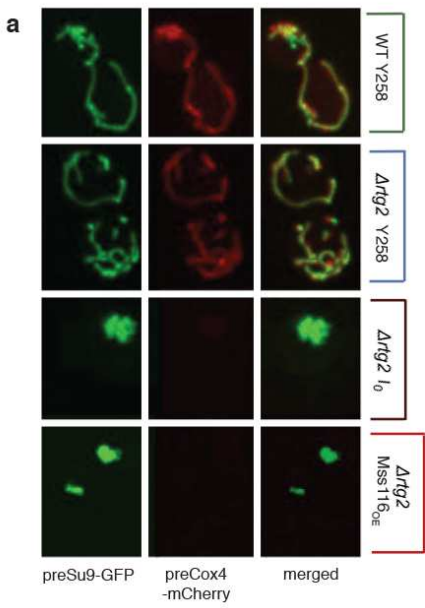
850

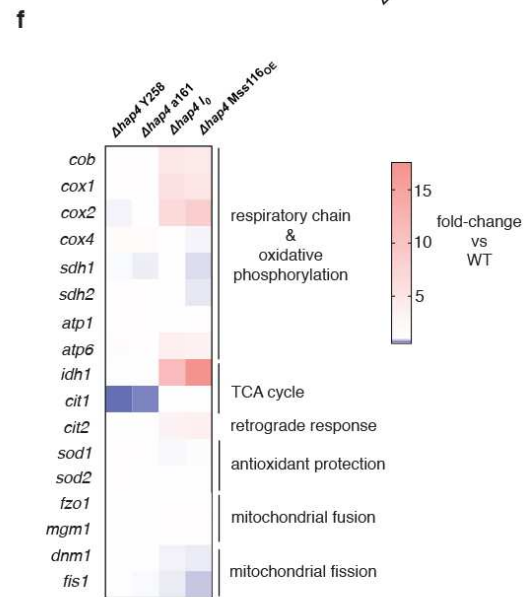
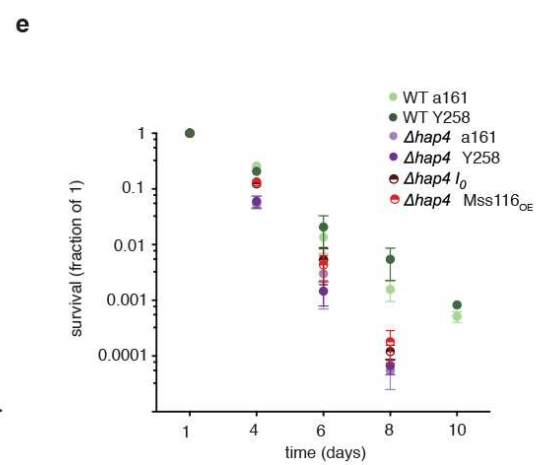
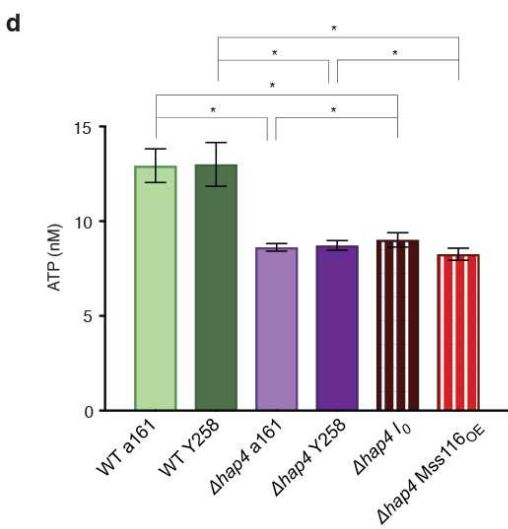
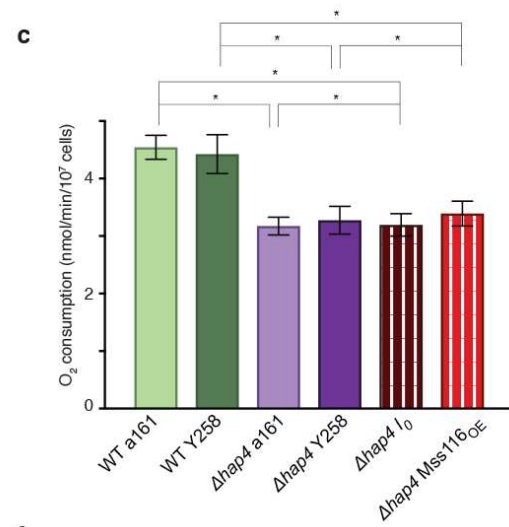
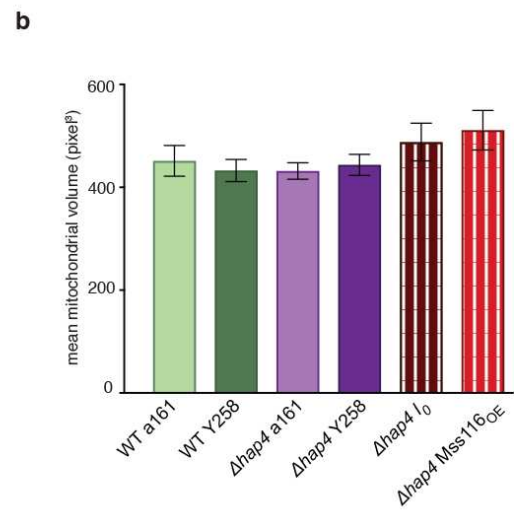
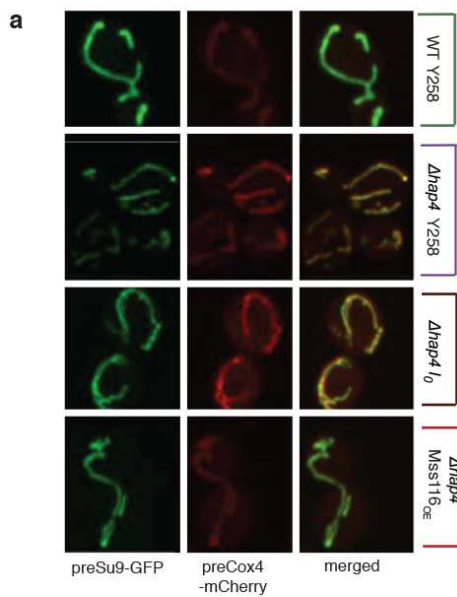
851

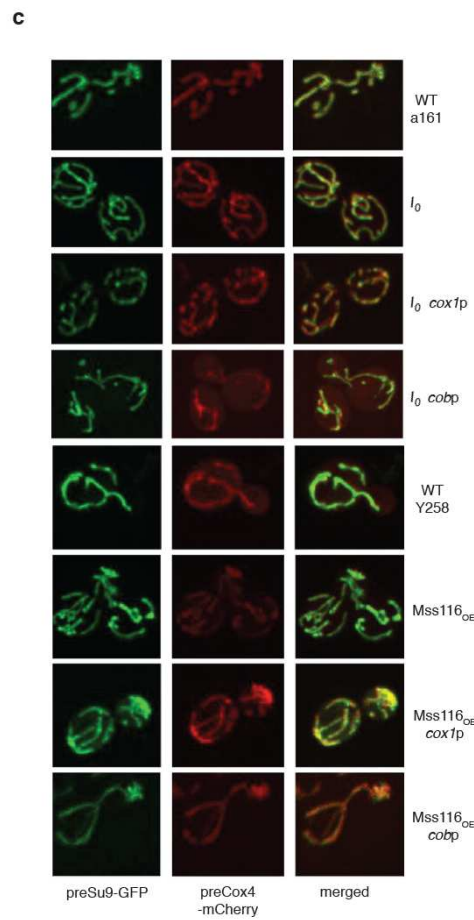
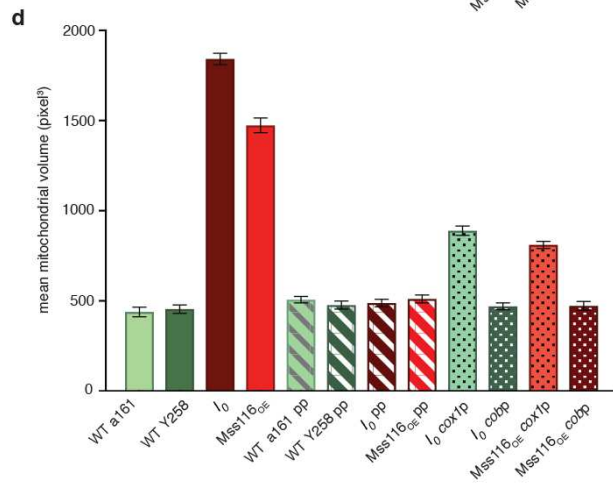
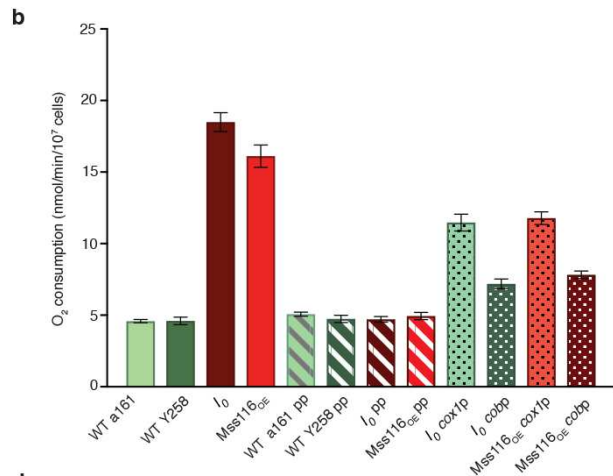
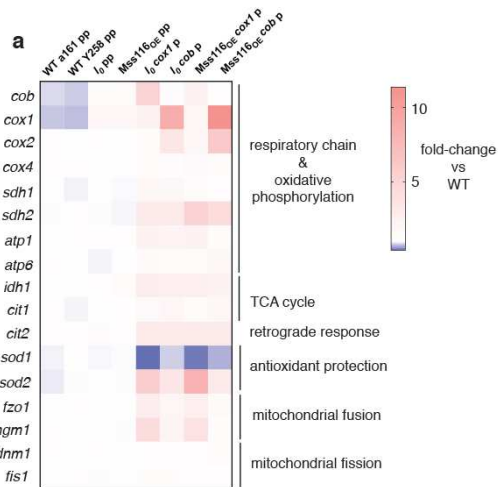
852

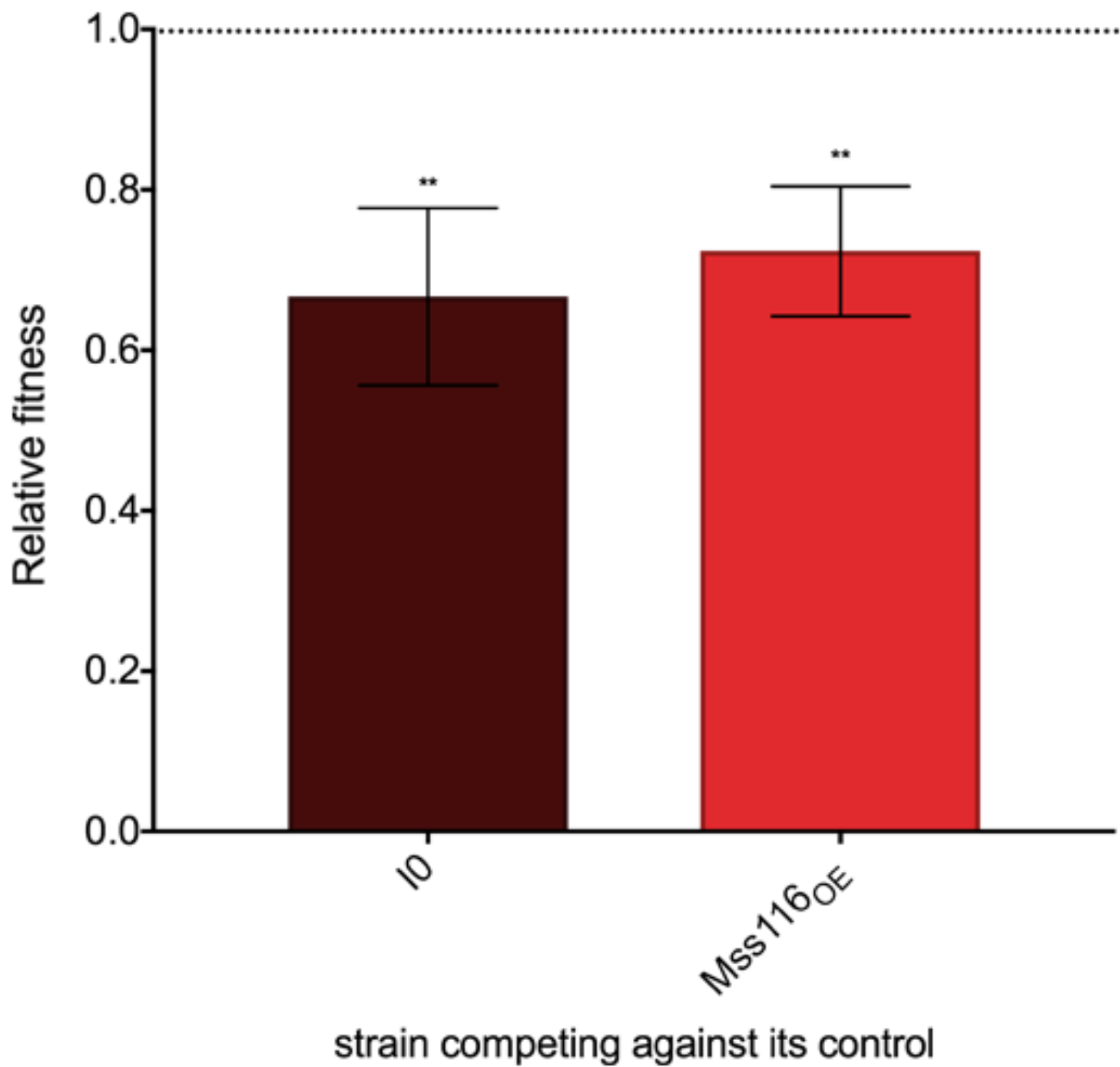






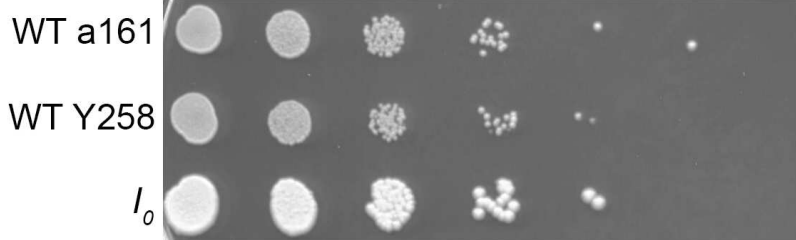






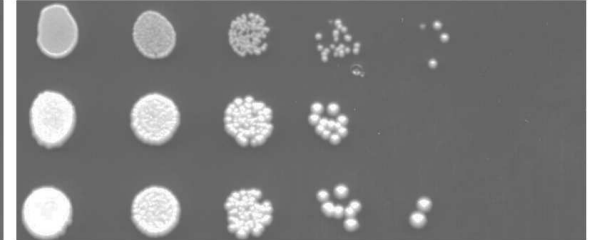
**a** 2% glucose

-1 -2 -3 -4 -5 -6

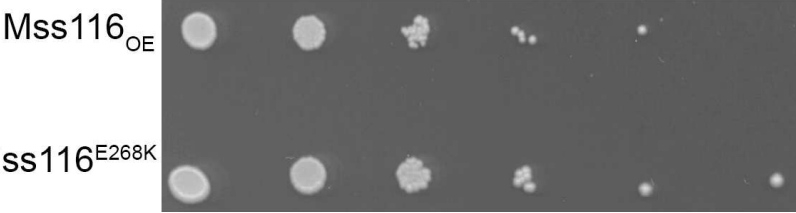


**b** glycerol

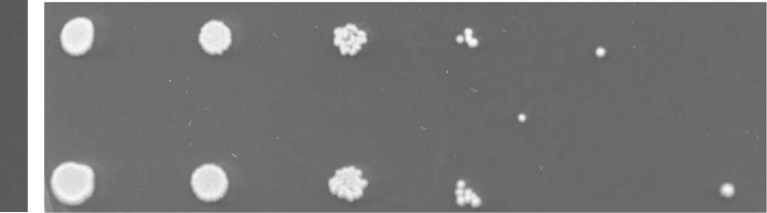
-1 -2 -3 -4 -5 -6



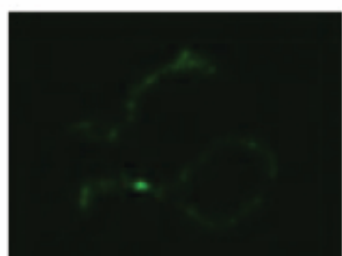
-1 -2 -3 -4 -5 -6



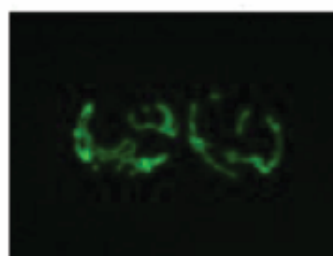
-1 -2 -3 -4 -5 -6



**a**

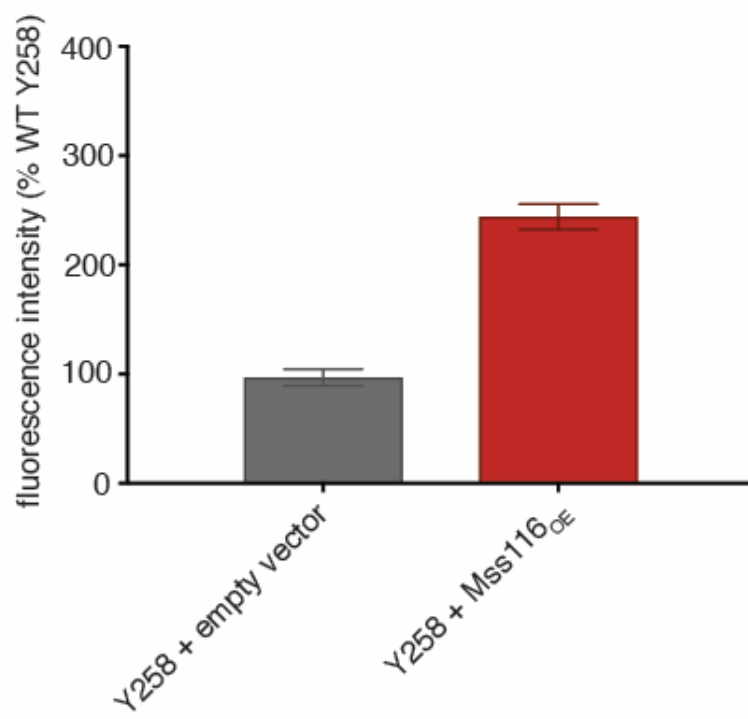


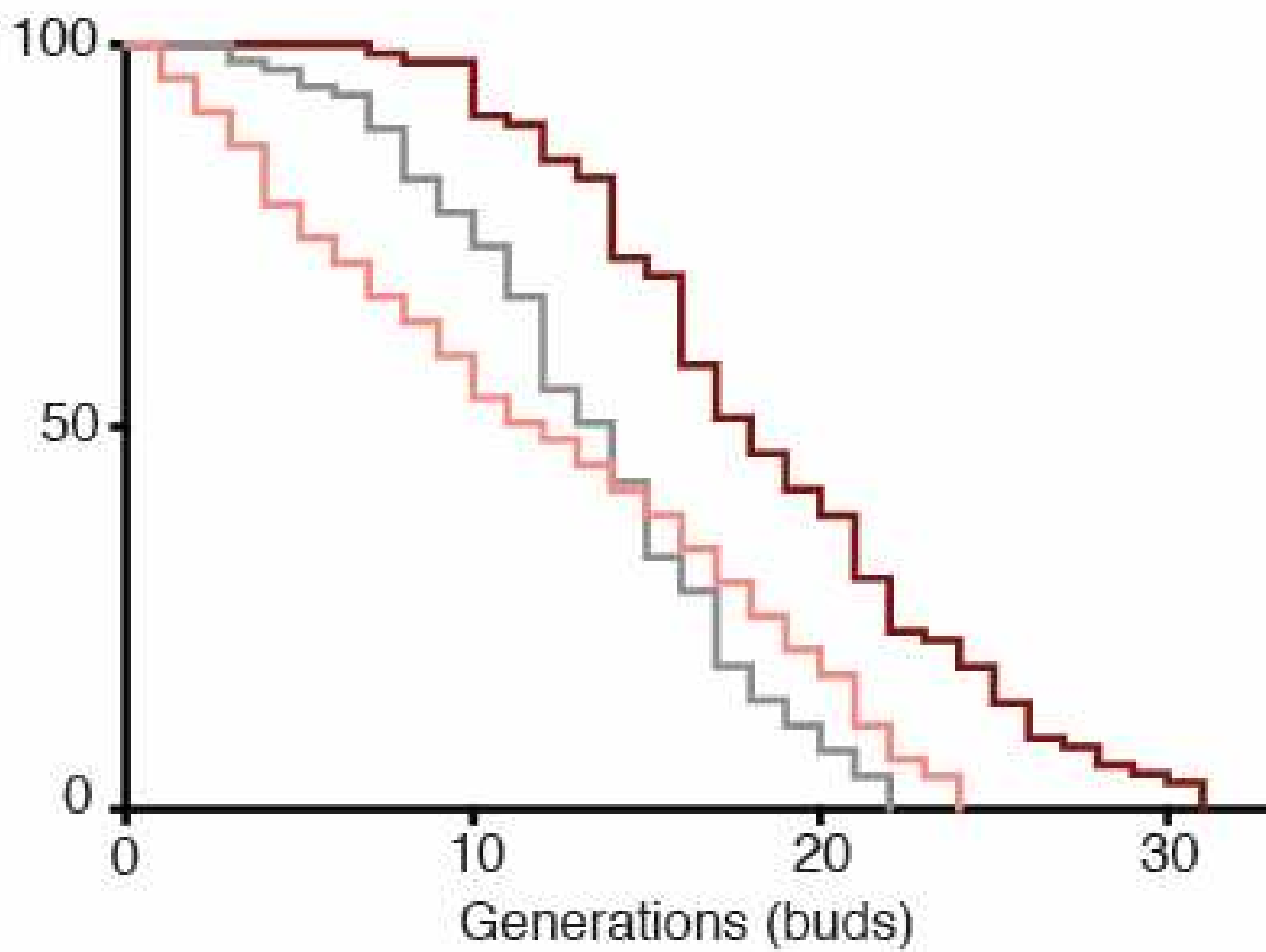
Mss116-GFP



ICC alpha-His-tag  
Mss116<sub>OE</sub>

**b**

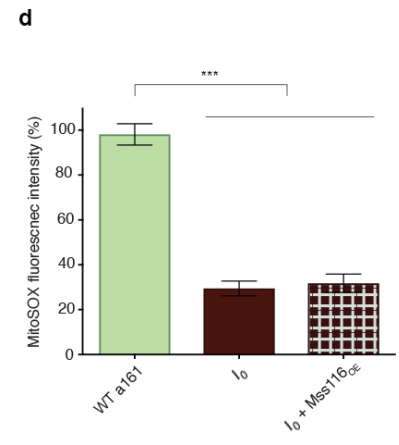
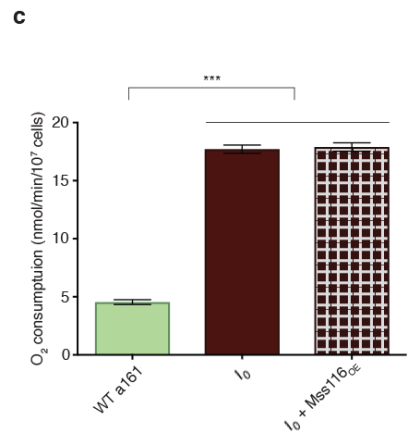
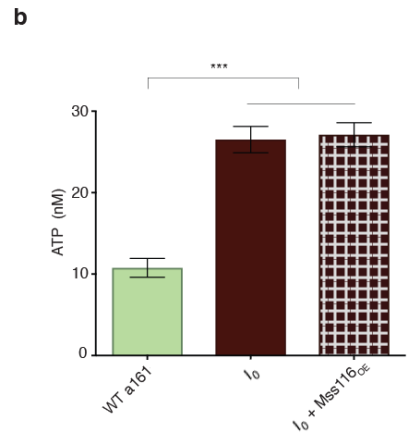
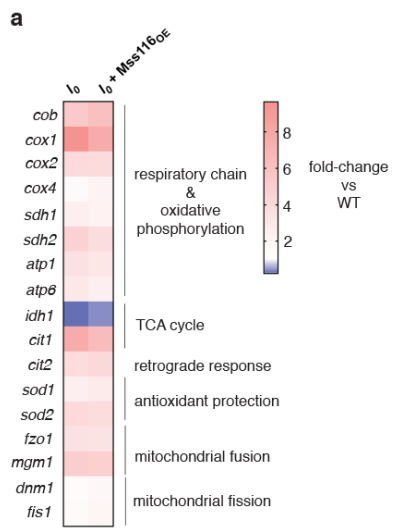


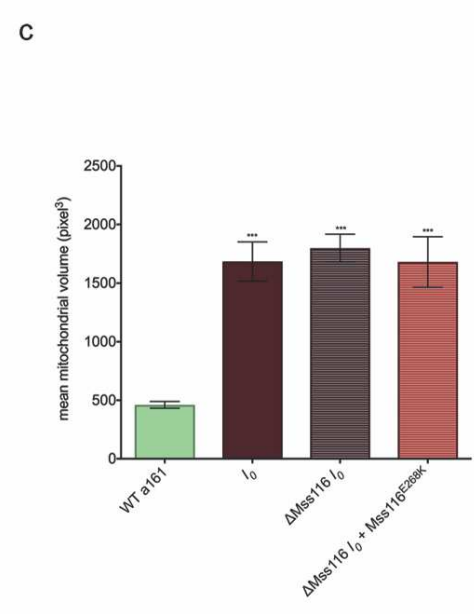
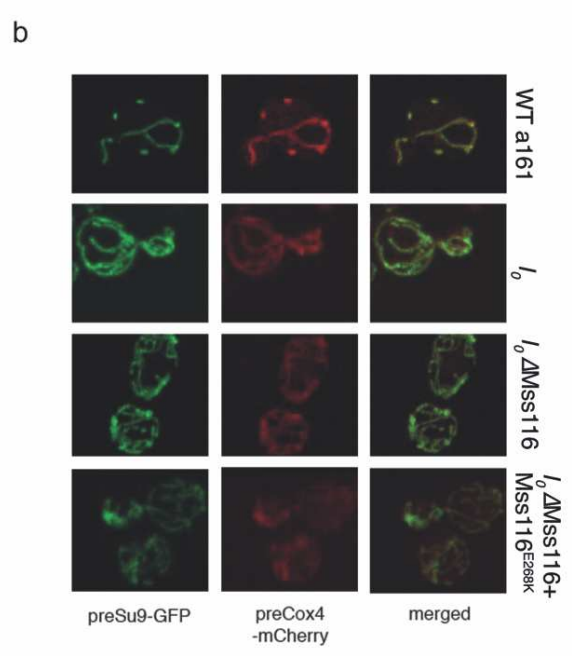
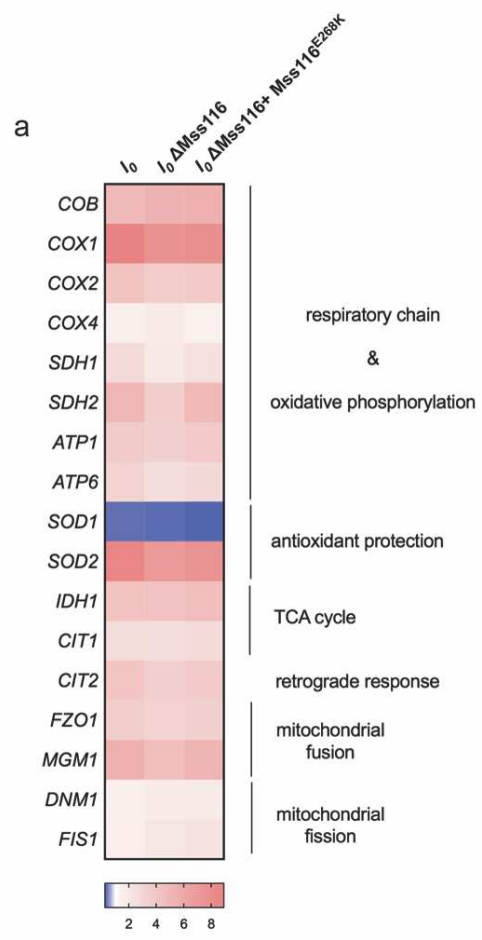


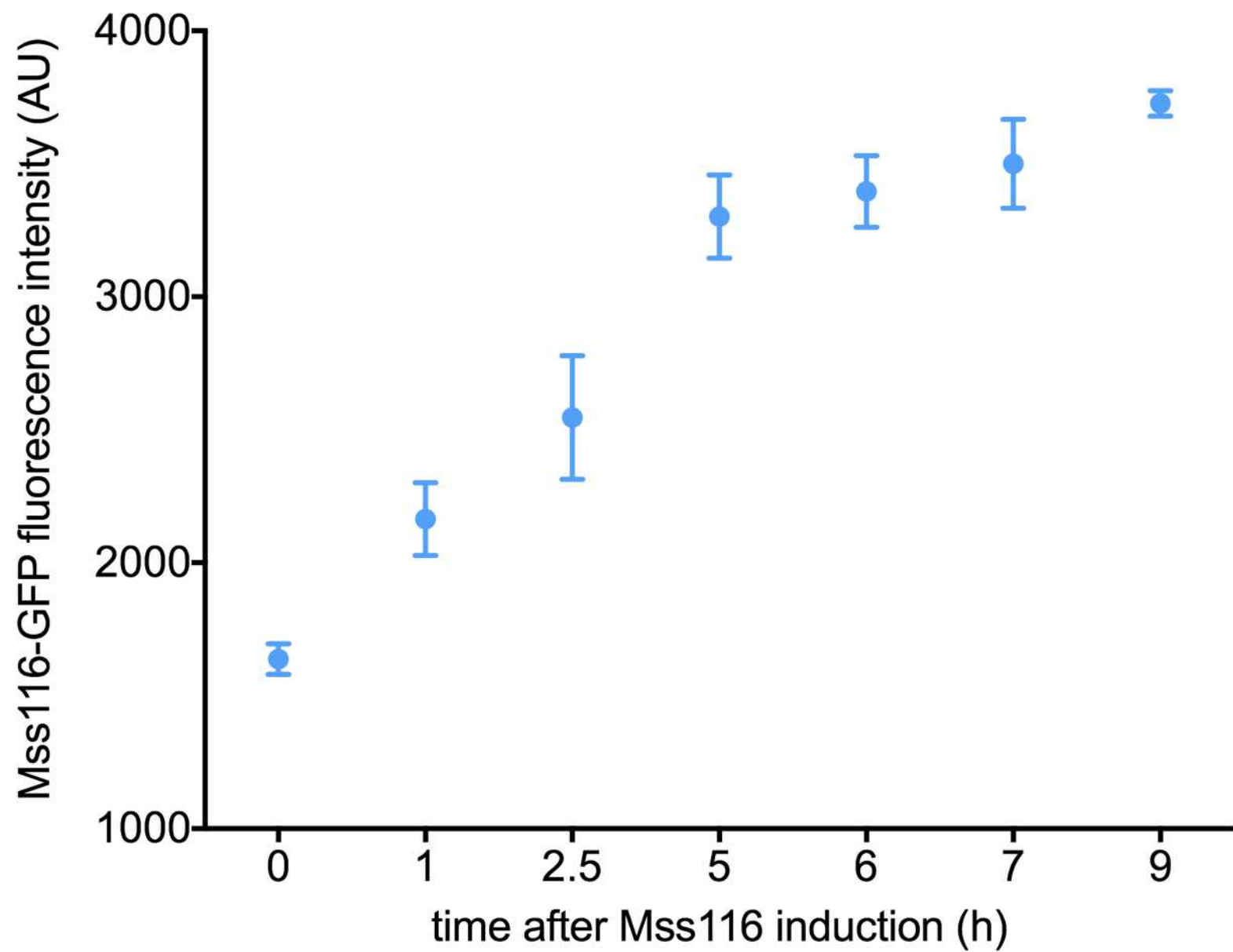
— WT Y258

— Mss116<sub>OE</sub>

— Mss116<sup>E288K</sup>



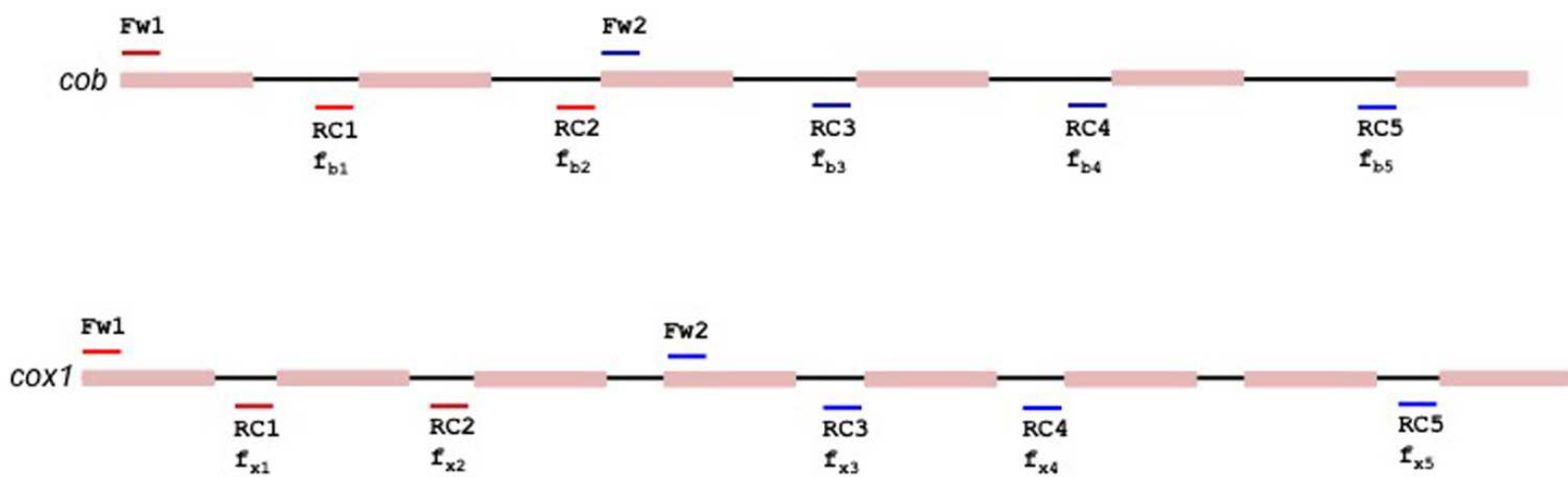




## mRNA



## pre-mRNA



*cox1* promoter

**ATTGATATAAGTAATAGATA**

↓  
**A**

beginning of *cox1* gene

**ATGGTACAAAGATGATTA**——

*cob* promoter

**TATTATATAAGTAATATATA**

↓  
**A**

beginning of *cob* gene

**ATGGCATTTAGAAAATCAAAT**——